A multi-model evaluation of aerosols over South Asia: Common problems and possible causes

Xiaohua Pan[1], Mian Chin[1], Ritesh Gautam [2], Huisheng Bian[1, 3], Dongchul Kim[1, 4], Peter R. Colarco[1], Thomas L. Diehl [1,4, *], Toshihiko Takemura [5], Luca Pozzoli [6], Kostas Tsigaridis [7, 8], Susanne Bauer [7, 8], Nicolas Bellouin [9]

1. NASA Goddard Space Flight Center, Greenbelt, MD, United States.
2. Indian Institute of Technology, Bombay, Mumbai, India.
3. University of Maryland Baltimore City, Baltimore, MD, United States.
4. Universities Space Research Association, Columbia, MD, United States
5. Kyushu University, Fukuoka, Japan.
6. Istanbul Technical University, Istanbul, Turkey.
7. NASA, Goddard Institute for Space Studies, New York, NY, United States.
8. Center for Climate Systems Research, Columbia University, New York, NY, United States.
9. Department of Meteorology, University of Reading, Reading, Berkshire, United Kingdom.

* Current address: European Commission at the Joint Research Center, Ispra, Italy

Correspondence to Xiaohua Pan (xiaohua.pan@nasa.gov)

Abstract

Atmospheric pollution over South Asia attracts special attention due to its effects on regional climate, water cycle and human health. These effects are potentially growing owing to rising trends of anthropogenic aerosol emissions. In this study, the spatio-temporal aerosol distributions over South Asia from seven global aerosol models are evaluated against aerosol retrievals from NASA satellite sensors and ground-based measurements for the period of 2000-2007. Overall, substantial underestimations of aerosol loading over South Asia are found systematically in most model simulations. Averaged over the entire South Asia, the annual mean aerosol optical depth (AOD) is underestimated by a range 15% to 44% across models compared to MISR, which is the lowest bound among various satellite AOD retrievals (from MISR, SeaWiFS, MODIS Aqua and Terra). In particular during the post-monsoon and wintertime periods (i.e. October-January), when agricultural waste burning and anthropogenic emissions dominate, models fail to capture AOD and aerosol absorption optical depth (AAOD) over the Indo-Gangetic Plain (IGP) compared to ground-based AERONET sunphotometer measurements. The underestimations of aerosol loading in models generally occur in the lower troposphere (below 2km) based on the comparisons of aerosol extinction profiles calculated by the models with those from CALIOP data. Furthermore, surface concentrations of all aerosol components (sulfate, nitrate, organic aerosol and black carbon) from the models are found much lower than in-situ measurements in winter. Several possible causes for these common problems of underestimating aerosols in models during the post-monsoon and wintertime periods are identified: the aerosol hygroscopic growth and formation of secondary inorganic aerosol are suppressed in the models because relative humidity is biased far too low in boundary layer, the nitrate aerosol is either missing or inadequately accounted for, and emissions from agricultural waste burning and biofuel usage are too low in the emission

inventories. These common problems and possible causes found in multiple models point out directions for future model improvements in this important region.

1. Introduction

South Asia, particularly the Indo-Gangetic Plain (IGP) bounded by the towering Himalaya that is conducive to trapping both anthropogenic and dust aerosols (Fig. 1), is one of the global hotspots with persistent high aerosol optical depth (AOD) routinely observed by satellite remote sensors (e.g. Moderate Resolution Imaging Spectroradiometer or MODIS, Multi-angle Imaging SpectroRadiometer or MISR and Sea-Viewing Wide Field-of-View Sensor or SeaWiFS), as well as from ground-based measurements (e.g. Aerosol Robotic Network or AERONET). The potential influence of aerosols on the climate and water cycle in this region (e.g. Indian summer monsoon) via surface dimming and atmospheric warming has been widely discussed in the literature (e.g. Ramanathan et al., 2005; Lau et al., 2006). The atmospheric heating due to absorbing aerosols (mainly from black carbon i.e. BC) is estimated to be large especially in the wintertime, about 50-70 W m^{-2} (Ganguly et al., 2006). Recent studies have shown that the depositions of absorbing aerosols such as BC and dust over Himalaya are linked to snow albedo reduction and accelerated snow/ice melt in Himalaya during the pre-monsoon season (Lau et al., 2010; Qian et al., 2011; Yasunari et al., 2010; Gautam et al., 2013).

Besides these climate impacts, fine aerosol particles ($PM_{2.5}$) are known to affect public health, especially over IGP where large portions of the Indian population live. At Delhi, for example, $PM_{2.5}$ concentration in 2007 was 97±56 μg/m^3 (Tiwari et al., 2009), nine times the air quality guidelines recommended by the World Health Organization in 2005. Increases in anthropogenic aerosol emissions and loading in South Asia in recent decades have been well documented (Ohara et al., 2007; Hsu et al., 2012; Kaskaoutis et al., 2012; Babu et al., 2013), in contrast with the decreasing emission trends over Europe and North America (Granier et al., 2011; Diehl et al., 2012). Therefore, it is critical to accurately represent aerosol sources, distributions and properties in models over this heavily polluted region in order to project the future climate and air quality changes in South Asia with confidence.

Previous studies, however, reported that global models generally underestimated aerosol loading over South Asia, especially over the IGP in winter (Reddy et al., 2004; Chin et al., 2009; Ganguly et al., 2009; Henriksson et al., 2011; Goto et al., 2011; Cherian et al., 2013; Sanap et al., 2014). Among them, Ganguly et al. (2009) reported that the GFDL-AM2 model largely underestimated the AOD over the IGP during winter by a factor of 6. Recently, AOD simulated by the regional climate model (RegCM4) showed higher correlation with AERONET AOD at stations over dust-dominated areas in south Asia than over the regions dominated by anthropogenic aerosols, i.e. 0.71 vs. 0.47 (Nair et al., 2012). Eleven out of twelve models participating in the Aerosol Comparisons between Observations and Models (AeroCom) phase I exercise were also found to underestimate the aerosol extinction over South Asia, especially under 2 km, in comparison with the space-borne lidar measurements from the Cloud–Aerosol Lidar and Infrared Pathfinder Satellite Observations (CALIPSO) satellite (Koffi et al., 2012).

The ability to capture surface BC concentrations over South Asia for models has also been found to be limited, with the low biases that tend to be larger in winter (Ganguly et al., 2009; Menon et al., 2010; Nair et al., 2012; Moorthy et al., 2013). A very recent study evaluating the latest generations of quasi-operational aerosol models participating in International Cooperative for Aerosol Prediction (ICAP) has shown that the models have very low skill scores in reproducing AERONET measured AOD at Kanpur, an urban city in northern India (Sessions et al., 2015). These studies underscore great challenges for current global aerosol models to adequately represent aerosols in South Asia.

Extending from previous studies and utilizing the recent model outputs from the AeroCom Phase II multi-model experiments, the present work systematically evaluates aerosol simulations in South Asia by seven global aerosol models with observations from satellites and ground-based measurements, and strives to characterize the model deficiency in reproducing observations. The outcomes of this study will help us understand the discrepancies between models and observations, thus providing directions for future model improvements in this important region.

The description of models is given in Section 2, followed by the introduction of observational data from satellites and ground-based measurements in Section 3. The model results are compared with observations in Section 4, including the spatial and temporal distribution of AOD and aerosol absorption optical depth (AAOD), vertical profile of aerosol extinction coefficient, and the surface BC concentration. The diversity among models is discussed in Section 5, and possible causes for the model underestimations of aerosol amounts are investigated in Section 6. Major findings are summarized in Section 7.

2. Model description

2.1 Models

Aerosol simulations for the period of 2000-2007 from seven models, including six models that participated in AeroCom Phase II hindcast experiment (i.e. AeroCom II HCA) and one additional model, GEOS5, are analyzed in this paper (see Table 1 for details). Note that the model outputs related to aerosol optical properties, such as AOD, AAOD and extinction coefficient, are at the wavelength of 550 nm. Given that MODIS and MISR are available only after 2000, we chose the years 2000-2007 in this study although longer time period of simulations (starting from 1980) are available from the AeroCom models (note that ECHAM5-HAMMOZ ended in 2005 and HadGEM2 in 2006). Aerosol modules in GEOS5 are based on GOCART with some modifications (Colarco et al., 2010). More detailed descriptions about these models can be found in previous studies (see references listed in Table 1 and Myhre et al., 2013). All models include sulfate (SO_4^{2-}), BC, organic aerosol (OA), dust (DU) and sea salt (SS). Nitrate (NO_3^-) is included only in three models (GISS-modelE, GISS-MATRIX and HadGEM2). The secondary organic aerosol (SOA) chemistry is resolved in two models, GISS-modelE and HadGEM2, whereas simple parameterizations of SOA are used in the remaining models. There are some differences among the seven models on aerosol optical properties (see refractive indices listed in Table 1). In comparison with satellite retrievals and AERONET observations that are available only under clear-sky conditions, it is desirable to use the

modeled AOD for clear-sky as well; however only two GISS models provide such output (other models just provide all-sky results). In general, clear-sky AOD is lower than all-sky AOD, for example, by 20% globally based on the GEOS-Chem model (Yu et al., 2012). All seven models use the assimilated wind fields although from different datasets. The horizontal resolutions vary from 2.8º by 2.8º (ECHAM5-HAMMOZ) to 1.1º by 1.1º(SPRINTARS) and the vertical levels range from 30 (GOCART-v4) to 72 (GEOS5) intervals. More information is given in Table 1.

2.2 Emissions

For anthropogenic emissions, which are mainly from consumption of fossil fuel and biofuel, the models use either A2-ACCMIP or A2-MAP emission dataset that are provided for the AeroCom Phase II model experiments (Diehl et al., 2012). Both A2-ACCMIP and A2-MAP were constructed by combining multiple inventories but in different ways. The annual anthropogenic emissions from A2-MAP are yearly emission dataset with inter-annual variability, while those from A2-ACCMIP are without actual inter-annual variability, simply generated by linear interpolation between decadal endpoints except for biomass burning (Granier et al., 2011; Diehl et al., 2012). Over South Asia, the spatial distribution and total emission amount are somewhat different between the two emission datasets, with higher emission amount in A2-ACCMIP. Detailed information on both emission datasets can be found in Diehl et al. (2012).

Figure 2 shows the averaged annual mean (2000-2007) anthropogenic BC, organic aerosol (OC), SO_2, NH_3 and NO_x emissions in South Asia from A2-ACCMIP anthropogenic emission dataset (A2-MAP is not shown and it does not provide NH_3 and NO_x emissions). In this study, we define the South Asia domain as 60°E–95°E longitude and 5°N –36°N latitude. Note that the seasonal cycle of anthropogenic emission is not resolved in either emission datasets, which could be problematic especially for biofuel emission in this region (discussed in Section 6.3). The anthropogenic emissions display high spatial heterogeneities over South Asia, coinciding with the population density distribution as reported by previous studies (e.g. Girolamo et al., 2004). Densely populated regions are usually associated with heavy anthropogenic emissions in South Asia, especially over IGP. The annual mean anthropogenic aerosols emission in South Asia for the period of 2000-2007 from A2-ACCMIP (A2-MAP) are 7.46 (5.33) Tg yr^{-1} of SO_2, 5.94 Tg yr^{-1} of NH_3, 4.50 Tg yr^{-1} of NO_x, 2.18 (1.71) Tg C yr^{-1} of OC, and 0.69 (0.65) Tg C yr^{-1} of BC. The ratio of OC/BC anthropogenic emissions (fossil fuel and biofuel) is 3.2 (2.6) over South Asia.

Open biomass burning including the agricultural residue burned in the field and forest fires contributes to 25% of total BC (and OC) emissions over India based on the estimation by Venkataraman et al. (2006) with the difference between the total crop waste and that used as fuel and animal fodder. Figure 3 shows the seasonal BC biomass burning emission based on monthly Global Fire Emissions Database Version 2 (GFED2), which is used by both A2-ACCMIP and A2-MAP emission datasets. The open biomass burning displays strong spatial and seasonal variations. Pre-monsoon period is the most active open biomass burning season with an emission amount of 0.22 Tg C yr^{-1} of BC over South Asia, concentrated over

northeastern India associated with the Jhum cultivation to clear the forest and create fields (Vadrevu et al., 2013). Seasonal practices of biomass burning of agricultural crop residues associated with rice-wheat crop rotation over the western IGP, such as Punjab, Haryana and western Uttar Pradesh, could explain the high aerosol loading during the post-monsoon of October-November (Badarinath et al., 2009a; Sharma et al., 2010; Vadrevu et al., 2011; Vadrevu et al., 2013) with a total emission amount of 0.001 Tg C yr^{-1} BC over South Asia in GFED2. The ratio of OC/BC open biomass burning emission is 8.0 averaged over South Asia.

The major natural aerosol over South Asia is the wind-blown mineral dust from the arid and semi-arid regions of southwest Asia, such as Iran, Afghanistan, Pakistan, Arabian Peninsula, and Thar Desert in the northwestern India. The dust emissions are calculated by each model and show a large diversity varying from 10.6± 3.3 (ECH) to 185.8± 33.6 (SPR) Tg yr^{-1} over South Asia (averaged for 2000-2007). This model diversity is attributed to differences in the model size bins of dust aerosols, parameterization of source strength, and wind fields and soil properties over source regions (see more detailed discussions in Section 5). Sea salt emission is negligible for the study area.

3. Observational datasets

3.1 Satellite data

In this study, five satellite products are used to characterize aerosol distribution and evaluate the model simulations. MODIS Terra and Aqua level-3 monthly mean AOD products at 550nm wavelength (Collection 5.1) are used by averaging the daily aerosol products at 1°×1° grid. The MODIS AOD is a composite of the Dark Target (Levy et al., 2007 and 2010) and Deep Blue retrieval products (Hsu et al., 2006), as the latter is able to retrieve AOD over bright surfaces such as the Thar Desert in South Asia. SeaWiFS level-3 monthly AOD products at 550nm (V003) are obtained by averaging the daily aerosol products at 1°×1° grid. SeaWiFS retrieval adopts the Deep Blue algorithm over land (Hsu et al., 2006, 2012) and Ocean Aerosol Retrieval (SOAR) algorithm over ocean (Sayer et al., 2012 and 2013). MISR level-3 monthly AOD products at 555nm (V004) are used by averaging the weekly aerosol products at 0.5°×0.5° grid. MISR retrieves aerosol properties over a variety of terrain including bright surface like deserts (Martonchik et al., 2004; Kahn et al., 2007 and 2010). In spite of the fact that the satellite data are instantaneous observations at local overpass times (varying between 10:30AM to 1:30PM for MODIS, MISR, and SeaWiFS) while models outputs are diurnally varying, any bias caused by diurnal vs. instantaneous sampling is expected to be small for monthly mean AOD. The study by Colarco et al. (2010) compared model simulated AOD sampled at MODIS/MISR overpass times with those averaged over diurnal time steps and found the differences to be small for monthly mean AOD, with only about 10% difference in south America and southern Africa (i.e. biomass burning regions) and smaller elsewhere.

The climatology (averaged over the period of June 2006-December 2011) of vertical extinction profiles from the Cloud-Aerosol Lidar with Orthogonal Polarization (CALIOP) layer product version 3.01(onboard CALIPSO satellite) is used to evaluate the model simulated aerosol vertical distribution in 2006 (CALIPSO 2011; Koffi et al., 2012). Only the CALIOP

observations in 532 nm channel for nighttime are used because of their better signal-to-noise compared to daytime observations. Three aerosol parameters are used to inter-compare model simulations with CALIOP, namely AOD, Z_a (km) and F_{2km} (%). AOD is the integral of extinction coefficient within the entire column (Eq.1). Z_a is defined as the averaged aerosol layer height (Eq. 2), and F_{2km} is defined as the percentage of AOD located in the lowest 2 km (Eq. 3) in the column.

$$AOD = \sum_{i=1}^{n} EXT_i \times \Delta Z_i \quad (1)$$

$$Z_a = \frac{\sum_{i=1}^{n} EXT_i \times Z_i}{\sum_{i=1}^{n} EXT_i} \quad (2)$$

$$F_{2km} = \frac{\sum_{i=1}^{level\ of\ 2km} EXT_i \times \Delta Z_i}{\sum_{i=1}^{n} EXT_i \times \Delta Z_i} \quad (3)$$

3.2 AERONET

In this study, we use AOD and AAOD data from the ground-based AERONET (Holben et al., 1998) sites in South Asia. Monthly mean AOD and AAOD were analyzed over Kanpur, Lahore and Karachi. Level-2 (version 2) data are used, which are cloud-screened and quality-assured aerosol products with a low uncertainty of 0.01–0.02. Locations of the three stations are shown in Fig.1 along with eleven in-situ measurement sites as described in the following Section 3.3. The information of all fourteen ground-based measurement sites is given in Table 2.

3.3 In-situ measurements

Modeled BC concentrations are also evaluated with the surface in-situ measurements from the Integrated Campaign for Aerosols gases and Radiation Budget (ICARB) field campaign in India over eight stations, which spread over Indian mainland and islands for the entire year of 2006. The BC data from ICARB field campaign were measured by inter-compared aethalometers following a common protocol. More details of ICARB measurements can be found in previous publications (e.g. Beegum et al., 2009 and Moorthy et al., 2013).

In order to examine the aerosol chemical composition (such as surface concentrations of nitrate, sulfate, organic aerosol and black carbon) and meteorological conditions (such as surface relative humidity and temperature) of winter haze over IGP in multi-models, we refer to measurements from the Indian Space Research Organization- Geosphere Biosphere Programme (ISRO-GBP) campaign which provided valuable information about aerosol physical, optical and chemical properties along the IGP during the wintertime of December 2004. For this study, four stations in IGP are selected because of their relatively complete measurements. They are Hisar (Ramachandran et al., 2006; Rengarajan et al., 2007; Das et al., 2008), Agra (Safai et al., 2008), Kanpur (Tripathi et al., 2006; Tare et al., 2006) and Allahabad (Ram et al., 2012a), from western to eastern IGP. Note that the in-situ data used in this study are obtained from the aforementioned references.

4. Results

In this section, the aerosol simulations by multi-models are evaluated in comparison to satellite data and ground-based measurements in terms of temporal variation and spatial distribution (horizontally and vertically) over South Asia.

4.1 Interannual variability of AOD

Figure 4a shows the annual averaged mean AOD over the entire South Asia domain (land only, shown in gray shaded area) for the period of 2000-2007. AODs are 0.270±0.008 and 0.273±0.012 from MISR and SeaWiFS (SeaW) retrievals respectively, and 0.326±0.010 and 0.332±0.018 from MODIS Aqua (MODIS-a) and Terra (MODIS-t) respectively. MISR AOD is the lowest bound of four satellite retrievals. The difference in AODs among satellite data is significant and could be up to 0.062 or 22% of MISR. Six out of seven models (except for HAD) consistently underestimated AOD by 0.043-0.119 or 15%-44% relative to MISR. As shown in Fig. 4b, over the central IGP region (77-83ºE/25-28ºN, denoted by the red box in Fig. 4a) where the hotspot of AOD is observed from satellites, the performance of the same six models are even worse, with the annual averaged mean AOD underestimated by 20-57% relative to MISR. Unlike other models, HAD shows comparable AOD with MISR and SeaWiFS over the entire South Asia (Fig.4a), but exceeds all satellite data over the central IGP (Fig.4b), higher than SeaWiFS and MISR by 47% and 58% respectively, and higher than MODIS-Terra and Aqua by 16% and 20% respectively. As shown in Figure 4a, the peak AOD in 2003 and the low AOD in 2005 appear in all satellite data (except MODIS Aqua in 2003), which are associated with the strength of dust emissions during the dry season in the same years (Kaskaoutis et al., 2012; Hsu et al., 2012; Ramachandran et al., 2013). However, all models fail to reproduce the peak AOD in 2003, whereas only two models (GE5 and SPR) indicate the low AOD in 2005.

4.2 Seasonal cycle of AOD and AAOD over 3 AERONET stations

To further examine the details of underestimations occurring in most models, we compare the model-simulated monthly variations of AOD and AAOD with the AERONET data at three selected sites in South Asia (Fig. 5). These locations represent different aerosol environments in South Asia: Kanpur, an industrial city located in the central IGP, is influenced by high anthropogenic emissions throughout the year and by the transported dust during pre-monsoon (MAM) and early monsoon periods (JJ); Lahore, an urban city located in the western IGP, is directly influenced by biomass burning in the pre-monsoon (MAM) and post-monsoon (ON) seasons; and Karachi, an urban coastal city in Pakistan, is influenced by frequent dust outbreaks, especially from the Arabian peninsula around early summer monsoon season (JJ). A two-year period is chosen for each site based on the availability of AERONET measurements. Three satellite datasets, namely MODIS-Aqua, MISR, and SeaWiFS, are also displayed to draw inter-comparison of AOD with AERONET data.

At Kanpur (first row of Fig. 5), strong seasonal variation of AERONET AOD (left column in Fig. 5) is evident with two peaks, one in May-July associated with dust outbreaks and the other in October-January associated with active open biomass burning as well as high

anthropogenic emissions. However, most models (except for HAD) only show the peak in May-July but miss the peak in October-January. Although the HAD model simulates two seasonal maxima, they disagree with the peak months observed from AERONET. Overall, AOD from all models have weak or negative correlation coefficients with AERONET data (from -0.34 to 0.34), with four models anti-correlated with AERONET data (ECH, GIM, GOC and HAD), and one with no correlation (GIE). AODs from six models are lower than those from AERONET as indicated by the relative biases ranging from 0.31 to 0.74. In contrast, HAD model overestimate the AOD by 44% (relative bias of 1.44). As for AAOD (right column in Fig. 5), models are much lower than the AERONET data by a factor of 2 on average, suggesting the underestimation of BC loading or weak aerosol absorption strength in models (see more analysis of BC in Section 4.5).

At Lahore (second row of Fig. 5), AERONET data are mostly available in the year 2007, when only five model results are available (no HAD and ECH for 2007, see Table 1). Lahore is located in the Punjab region, which is an agriculture region known as the ‘‘breadbasket’’ for Pakistan and India. The enhanced AERONET AOD and AAOD are evident at Lahore during October-November, which is linked to the agricultural waste burning after harvest. However, all five models largely underestimate AOD and AAOD in the October-November period. This suggests that emissions from agriculture waste burning are likely underestimated in GFED2 that are used by the models (discussed in Section 6.4). Compared to observations, HAD again showed abnormal seasonal variation at Lahore, similar to that at Kanpur, with extreme high AOD in October though.

At Karachi (third row of Fig. 5), a unimodal seasonal distribution is revealed in AERONET AOD data, in contrast to the bimodal seasonal variation at Kanpur. The maximum AOD around July is associated with the wind-driven mineral dust from the Arabian Peninsula, which is captured by the models as indicated by relatively strong correlation from 0.58 to 0.91 (except HAD. Note ECH is not available for 2006-2007). However, similar to other sites, AOD from all models are too low in late autumn to winter. Models also fail to capture the relatively higher AAOD around November that is associated with smoke transported from agriculture waste burning in northwestern IGP (i.e. the area around Lahore) (Badarinath et al., 2009a,b).

Overall, in comparison with AERONET at three sites, most models tend to significantly underestimate AOD in October-January when aerosols from agriculture waste burning and anthropogenic activities are dominant. On the other hand, the monthly variations and magnitudes of AOD from the satellites are in general similar to those from AERONET. As an exception, MODIS-Aqua is biased high (up to a factor of 2) during pre-monsoon and monsoon months. This overestimation of AOD partially results from low bias of surface reflectance under dusty conditions in the MODIS Dark-Target aerosol retrieval algorithm (Jethva et al., 2009).

In order to diagnose the discrepancies between models and AERONET data, the individual component AOD from four models (HAD, GE5, SPR and GOC, unavailable from other three models) are examined at Kanpur for 2004 in Fig. 6. We choose the year of 2004 because ISRO-GBP campaign took place in the same year (see Section 3.3 and Section 6), so that we can intercompare AERONET data with that in ISRO-GBP campaign. In December and

January, AOD from AERONET data is around 0.7, dominated by anthropogenic contributions (about 75%, estimated by Tripathi et al. 2006). All four models have difficulties to capture the magnitude of AOD in December and January. Among them, AOD from HAD (upper left panel in Fig. 6) matches relatively well with AERONET data, capturing about half of the observed value. Interestingly, nitrate (NO_3^-) AOD is the major component in HAD, contributing to 50% of total modeled AOD. In contrast, three other models (SPR, GE5 and GOC) largely underestimate the peak in the winter (December and January) by up to a factor of 7. As a common problem, these three models do not include the nitrate aerosol component. During the months of May to July, coarse mode aerosol (i.e. dust) contributes mostly to total AOD (> 60%) based on studies with ground based sun/sky radiometer data (e.g. Srivastava et al., 2012a). SPR and GE5 capture this feature while HAD and GOC underestimate the contribution of dust. In the HAD model, AODs from nitrate alone during April and October are comparable to column total AERONET AOD, indicating a problem in representing seasonal variation of nitrate in HAD, as shown in Fig. 5. Instead, nitrate aerosol is expected to peak in winter because of high relative humidity and low temperature over IGP that favor the formation of NH_4NO_3 (Feng and Penner 2007; Ram et al., 2010b; Ram et al., 2012b).

Overall, Fig. 6 demonstrates that the magnitudes and seasonal cycles of aerosol compositions are quite different across the models. Further examination of the model diversities will be discussed in Section 5.

4.3 Spatial distribution of AOD in different seasons

In this section, we compare the spatial distributions of AOD over the entire South Asia and neighboring oceans among four satellite products (MODIS-Terra, MODIS-Aqua, MISR, and SeaWiFS) and seven model simulations during the winter monsoon (DJF), pre-monsoon (MAM), summer monsoon (JJAS) and post monsoon (ON) phases averaged over 2000-2007, shown in Fig. 7a-b. Locations of the three aforementioned AERONET stations are also labeled in the maps for reference. In general, the spatial distribution of AOD is closely associated with the emission source over South Asia, and the aerosol abundance in the atmosphere is modulated by meteorological conditions, such as efficient atmospheric dispersion associated with the strengthened westerly flow in March-July, high wet removal associated with the monsoon rainfall in June–September, and stable atmospheric conditions and thus less efficient atmospheric dispersion in December-February.

During the winter season (DJF), local anthropogenic sources dominate over dust, contributing as much as 80% (±10%) to the aerosol loading (Ramanathan et al., 2001; Tripathi et al., 2006). The maximum AOD is found in the central and eastern IGP based on four satellite datasets as shown in Fig. 7a, which coincides with clusters of coal-based large thermal power plants (capacity >1970 MW) (Prasad et al., 2006). The natural topography (i.e. gradually decreased elevation eastward but narrow opening to the Bay of Bengal as shown in Fig. 1) is conducive to the accumulation of aerosol over central and eastern IGP. Additionally, the winter season is characterized by relatively stable atmospheric conditions that traps pollutants in the shallow atmospheric boundary layer (ABL), leading to strengthened hazy

conditions in the IGP (Girolamo et al., 2004; Gautam et al., 2007). The outflow of aerosols to the Bay of Bengal is clearly depicted by satellite data. As shown in the first column of Fig. 7b, however, only the HAD model shows the observed spatial pattern and magnitude of AOD, although it overestimates AOD over eastern IGP. Other models greatly underestimate the high AOD over IGP by 50% on average. In addition, the observed north-south gradient of AOD is not captured by most models, with SPR showing no gradient and ECH and GIM showing opposite gradient. The model underestimation over the Indian subcontinent in winter is probably owing to missing aerosol species such as nitrate aerosol suggested by Fig. 6, incorrect meteorological fields such as air temperature and relative humidity, or the underestimation of anthropogenic emissions (discussed in more details in Section 6).

Starting from the pre-monsoon season (MAM), the entire South Asia is characterized by high AOD mainly due to the mineral dust transported from the arid and desert regions in southwest Asian dust sources by westerly winds, with maximum AOD over western IGP seen from most satellites (Fig. 7a). As shown in the second column of Fig. 7b, five models (GOC, SPR, GIM, GIE and GE5) partially capture this observed spatial distribution and magnitude. However, the HAD model shows high biases of AOD over northern India due to nitrate (refer to Fig. 6). A higher nitrate concentration than dust is unrealistic because the contribution of dust to the total AOD has been reported to be over 60% during pre-monsoon season by Srivastava et al. (2012a) based on the ground based sun/sky radiometer data. The dust source in the northwestern parts of South Asia is weak in HAD (Fig. 7b). Additionally, the ECH model shows very low AOD and little dust over IGP associated with its small dust size in coarse mode (Table 1). Despite these deficiencies, model simulations over South Asia during the pre-monsoon season are still closer to the satellite data than those during winter, with the model-averaged AOD capturing 65% of the satellite data in the pre-monsoon season compared to only 50% in winter.

During the monsoon season (JJAS), dust transported from the Arabian Peninsula by the strong southwesterly winds explains the high AOD over northwestern India. High AOD over the Arabian Sea and southwest Asia is evident in MODIS and MISR (Fig. 7a). As shown in the third column of Fig. 7b, most models reproduce both the spatial distribution and the magnitude of AOD during this season, implying that these models capture dust emission over the Arabian Peninsula and its transport to South Asia. However, it should be noted that during the monsoon season the monthly mean AOD from MODIS is likely to be biased high as shown earlier in Fig 5, partly due to underestimated surface reflectance.

During the post-monsoon season (ON), the southwesterly flow significantly weakens, and thus dust transported to the Indian subcontinent is lower compared to the pre-monsoon and monsoon seasons. Based on the spatial distributions from satellite data (Fig. 7a), high AOD is found along IGP with maxima over western IGP including Punjab, Haryana and western Uttar Pradesh that are associated with biomass burning from agriculture waste fires. With the aid of northwesterly winds, aerosols are transported to the central IGP along the valley as well as the region to the south (Badarinath et al., 2009a, b). However, none of the models capture these features (the fourth column of Fig. 7b), indicating the biomass burning

emissions are severely underestimated in the current inventory based on GFED2, which will be discussed further in Section 6.4. In contrast to the underestimations by other models, HAD overestimated AOD over IGP due to the high amount of nitrate (Fig. 6).

4.4 Aerosol vertical distribution

Figure 8 shows the comparison of aerosol extinction profile among models and with CALIOP data in four seasons. In order to represent the latitudinal gradient of aerosol vertical profiles, two locations are chosen, Kanpur in northern India and Hyderabad in central India (refer two locations to Fig. 1). The CALIOP aerosol extinction profile over Kanpur (Fig. 8a, 2º x 2º box averaged around the station location) reaches a maximum value of 0.4 km^{-1} at the altitude < 1 km during winter (Z_a=1.18 km) but decreases rapidly upward and diminishes around 4 km. Note that low values near the surface (within 180 meters) in CALIOP profiles are likely due to the contamination by the surface return (CALIPSO, 2011; Koffi et al., 2012). In contrast with the relatively stable lower troposphere in winter, boundary layer mixing, convection, and transport are strengthened in pre-monsoon season. As a result, aerosols are more efficiently mixed vertically, with Z_a from CALIOP almost doubled from the season of DJF to MAM (from 1.18 to 2.18 km). The aerosol vertical mixing is relatively uniform within the lowest 2 km and extends to higher altitude around 6 km in MAM. The aerosol extinction near the surface in MAM is only 60% of its DJF values with the fraction of AOD in the lowest 2 km reducing from 84% in DJF to 52% in MAM. The aerosol profile during monsoon season (JJAS) is similar to that in pre-monsoon period but with a slightly lower value of Z_a as 2.02 km; and the profile during the post-monsoon is similar to that in the winter but with a slightly higher value of Z_a as1.24 km.

Most models, especially GE5, capture the observed seasonal variation of Z_a (and F_{2km}) over Kanpur, with lower Z_a (higher F_{2km}) during wintertime (DJF) and post-monsoon season (ON), while higher Z_a (lower F_{2km}) during the pre-monsoon (MAM) and monsoon seasons (JJAS). The profiles and magnitude in models, however, are quite different from those of CALIOP. At Kanpur in DJF, most models (except for HAD and GIE) largely underestimate AOD by 59% (ECH) to 85%(SPR), consistent with the preceding results (Fig. 5-7). In particular, the extinction coefficient in the lowest 2 km is largely underestimated, with F_{2km} varying from 68% (GIM) to 87% (GE5) among these five models in contrast to 84% in CALIOP (Fig. 8a). At Hyderabad in central India (Fig.8b), models agree better with the CALIOP during the winter (DJF) and post-monsoon (ON) seasons. At both stations, models agree better with CALIOP during the dust-laden pre-monsoon (MAM) and monsoon (JJAS) seasons than during two other seasons, consistent with the results in Fig.7a-b. There are some extremes of model simulated vertical profiles. For example, HAD produces extremely high extinction coefficients close to the surface at Kanpur throughout all seasons that are a factor of two greater than CALIOP in the season of DJF and a factor of ten greater in ON; GIE and GIM are greater than CALIOP by a factor of four and seven close to the surface in JJAS, respectively; and GIE exhibits extremely large extinction coefficients between 2 and 3 km in all seasons, which is not found in CALIOP.

4.5 Monthly BC surface concentration

Figure 9 shows the observed and modeled monthly surface BC concentration in the year of 2006 (2005 from model ECH) at eight ICARB stations (refer the locations to Fig.1). In general, the magnitude of BC surface concentrations is closely related to the strength of emission source, with higher values in northern India where higher BC anthropogenic emissions are located (refer the spatial pattern to Fig.2). The highest BC surface concentration is particularly found in the largest Indian city Delhi, with a value of 27μg m^{-3} in January. In contrast, BC surface concentration is lower in the remote sites, such as the island sites (Minicoy and Port Blair) and mountain site (Nainital), not exceeding 2.8μg m^{-3}. The observed surface BC concentration exhibits pronounced seasonal variation with higher values found in the winter and post-monsoon seasons and lower values in the spring and summer, which can be attributed to the seasonal variations of emission, atmospheric boundary layer (ABL) depth (affecting vertical mixing), and rainfall (removing BC from the atmosphere). It was reported by previous studies that total BC loading over South Asia mainly resulted from biofuel emissions in winter along with coal burning in the vicinity of the measurement location (e.g. Ali et al., 2004; Singh et al., 2008; Beegum et al., 2009; Srivastava et al., 2012b). In comparison with observation, modeled BC surface concentrations at all stations except Nainital (a mountain site) and Kharapgpur are too low, especially in winter. In particular, at Delhi and Hyderabad - two very large cities with populations of 16.75 and 6.81 million respectively (Table 1), all models show a pronounced low bias in the winter, capturing only 3%-19% of the observed values. As a matter of fact, the models have difficulties to reproduce the observed high pollution levels only near the emission sources such as urban cities (e.g. Delhi and Hyderabad), but also in more remote locations (e.g. over the mountain site of Nainital and the island sites of Minicoy and Port Blair). At Minicoy and Port Blair, where the observed BC concentrations are relatively low, models capture only about 10%-38% of the observed values. In addition to the fact that modeled AODs were also found to be significantly low in comparison with both AERONET point observations and with the multiple gridded satellite data from MODIS, SeaWiFS (both 1˚x1˚ resolution) and MISR (0.5˚x0.5˚ resolution) on regional scales, as shown earlier in Fig. 5 and Fig. 7, the underestimations of modeled BC and AOD in winter are more likely due to other factors than coarse model resolution, which will be discussed in details in Section 6. As an exception, the simulated BC surface concentrations are found to have a better agreement at Kharagpur, a semi-urban city with populations less than 1 million, where models capture 20%-100% of the observed value. This contrast with other stations is possibly attributed to the fact that BC loading at Kharagpur mainly comes from coal-fired power plants (Nair et al., 2007), which are likely well represented in the emission data (discussed further in Section 6.3).

5. Model diversity

Clearly, there is a large diversity existing among models in simulating AOD and BC concentrations as shown in Fig. 4-9, despite similar emission datasets used in these models (see Section 2.2 and Table 1). It is seen that models with the same emissions datasets

produce quite different results. For example, at Kharagpur, shown in the upper right panel of Fig.9, the surface concentration of BC from the SPR model is four times as large as that from GIM, although both models use the same anthropogenic emission (A2-ACCMIP) and biomass burning emission (GFED2). Similarly, surface concentration of BC in the HAD model is twice as that of GOC, although the same emissions (A2-MAP and GFED2) are used in both models. Such substantial differences indicate that the large diversity among model simulations is due to factors other than the differences in emissions. Textor et al. (2007) also found that the differences in the model treatment of atmospheric processes (e.g., wet removal, dry deposition, cloud convection, aqueous-phase oxidation and transport), assumptions of particle size, mixture, water uptake efficiency, and optical properties are more responsible than emission for the model diversity. More recently, Bond et al. (2013) pointed out that large differences in modeled horizontal and vertical transport are mostly responsible for the inter-model diversity of BC distributions.

The multi-model diversity (defined as the percentage of the standard deviation to the mean of results from the seven models) over South Asia in 2006 (2005 from the model ECH) is summarized in Table 3 (also demonstrated in supplement Fig. S1-3). In general, on an annual basis, we found the following features: (1) For aerosols with anthropogenic origin (i.e. BC, OA and SO_4), the diversity of dry deposition among models is large, with diversity ranging from 41% to 46% across these three species. Correspondingly, the fraction of dry deposition to total deposition shows 29-40% diversity for the same three species. In contrast, the diversity of wet deposition is relatively smaller with a range from 15 to 22% across these three species. The chemical production of sulfate in gas phase among models (four models) has large diversity about 66%. (2) For mineral dust, the emission itself has very large diversity among the models about 124%, leading to a similarly large diversity of dry deposition (aerodynamic dry deposition + gravitational settling) of 115%. The difference of treatment of dust size bin in models contributes significantly to these diversities (see Table 1). In contrast, diversity of dust mass loading and AOD are much smaller at 45% and 22% respectively. (3) BC has the largest model diversity of mass extinction efficiency (MEE) at 51%, compared to 25% and 27% for SO_4 and OA respectively.

We further examine the aerosol refractive index at 550nm for each species as listed in Table 1. The real part of refractive indices at 550nm is similar among the seven models, but the imaginary part (representing light absorption) is different. In the case of BC, the most absorbing aerosol, its imaginary refractive index is 0.44 in four models and 0.71 in three models, which are lower than the value of 0.79 recommended by Bond and Bergstrom (2006). For dust, the light absorption at 550nm is significantly less than that of BC. The imaginary refractive index of dust ranges from 0.001 (ECH) to 0.008 (GE5), a range that is much wider than that of BC. The differences in the absorption properties, together with the differences of model simulated BC and dust amount, contribute to the diversity of model calculated AAOD at 37%.

6. Possible causes of model underestimation of aerosols over South Asia

As shown in Section 4, AOD, AAOD and BC surface concentration over South Asia are consistently underestimated in seven global models used in this study, in particular during winter and the post-monsoon season. Such underestimation seems to be a common problem in other models as well (e.g. Reddy et al., 2004; Ganguly et al., 2009; Nair et al., 2012). AOD and surface BC concentrations are most severely underestimated over the IGP (the main region of anthropogenic emissions). Several possible causes for these underestimations are suggested below.

6.1 Wintertime relative humidity (RH) over the IGP

Foggy days with high near-surface relative humidity are very common during wintertime over IGP (Gautam et al., 2007). For example, Kanpur was subjected to heavy fog or haze for about >65% days in December 2004, with averaged surface RH of about 75% and the surface temperature about 14.6ºC (Tripathi et al., 2006). Low precipitation and thus low wet removal in winter further contributes to accumulation of aerosols (Tripathi et al., 2006).

Figure 10 shows comparisons between models and in-situ measurements (ISRO-GBP land campaign) at four stations located in the IGP region in December 2004. Comparisons are shown for surface meteorological conditions (RH and temperature); surface aerosol concentrations of SO_4^{2-}, NO_3^-, OA and BC; and columnar AOD and AAOD. AODs from the models are only 10% to 50% of the observed values at Kanpur. Interestingly, we found that RH in six of the seven models (except for HAD) only range from 11 to 35% at Kanpur, much lower than the measured RH of 75% (first row, Fig. 10). This large underestimation of RH could be partly due to the warm bias of air temperature by 1.7-7.5 ºC across models (second row, Fig. 10) and thus high bias of saturation water vapor pressure and low bias of RH. Under such dry conditions in models, the hygroscopic growth of soluble aerosols is consequently suppressed. Averaged over these four IGP stations, for example, if RH is improved from the modeled 21% to the observed 66%, mass extinction efficiencies (MEE) of SO_4^{2-} would be doubled, and those of OC and NO_3^- would be enhanced by 50% (Fig. 11). It is interesting that the HAD model, in which the simulated AOD matches observed one relatively better, is the only model with high bias of RH.

In addition to favor hygroscopic growth, foggy conditions also favor the formation of secondary inorganic aerosol through the aqueous-phase reactions. This phenomenon was supported by the observations of increased aerosol number concentration and surface SO_4^{2-} concentrations under foggy conditions at Kanpur (Tare et al., 2006), Hisar and Allahabad (Ram et al., 2012a). High RH and lower temperature in winter also favor the formation of NH_4NO_3 by the reaction of nitric acid (HNO_3) with NH_3 (Feng and Penner 2007; Ram et al., 2010b; Ram et al., 2012b). However, the lack of representing foggy conditions in current models, which is indicated by the low bias of RH, would suppress these reactions in winter. Hence, it is not surprising that the surface mass concentrations of SO_4^{2-} and NO_3^- in models are found to be much lower than the observed values. As shown in Fig. 10, all models underestimate the surface concentration of SO_4^{2-}, with capturing merely from 5% (GIE and GIM) to 50% (GE5) of the observed value. SO_4^{2-} concentration, however, is found low in HAD as well although with

high relative humidity. The specific reason is unclear yet. Among three models that include NO_3^-, GIE and GIM produce extremely low NO_3^- concentrations that are only 0.1% of the observed amount, whereas HAD captures about 38% of the observation. The model underestimations of surface aerosol concentrations might be caused by other factors as well, such as unaccounted for anthropogenic emissions (see section 6.3) or insufficient oxidant amounts (H_2O_2 and OH); however, the lack of representing foggy conditions or the low bias of RH in the models appears to be a critical factor contributing to the overall underestimation of aerosols.

6.2 Nitrate component

As shown in Fig. 10, the observed surface concentrations of NO_3^- are comparable to or even higher than those of SO_4^{2-} at four stations (e.g. 14.9 μg m^{-3} of SO_4^{2-} and 15.7 μg m^{-3} of NO_3^- at Kanpur, and 14.1 μg m^{-3} of SO_4^{2-} and 31.4 μg m^{-3} of NO_3^- at Agra). However, NO_3^- is either missing in the models (GOC, ECH, SPR, GE5) or much too low (especially in GIE and GIM). Interestingly, AOD is closer to observations in the HAD model than in other models, which is not only apparent at 4 stations in IGP (Kanpur, Agra, Allahabad and Hisar) (Fig. 10) but also over entire South Asia (Fig. 7b). Such agreement is partly associated with its inclusion of NO_3^- (Fig. 6) and aforementioned high relative humidity in winter (Section 6.1). This study underscores the importance of NO_3^- to adequately represent the total AOD over South Asia.

6.3 Anthropogenic/Biofuel emission amounts and seasonal variation

The uncertain and inadequate representations of aerosol emissions over South Asia have been pointed out by previous studies (e.g. Sahu et al., 2008; Ganguly et al., 2009; Nair et al., 2012; Lawrence and Lelieveld, 2010). The results in this study further prove this issue. At Kanpur, the models underestimate not only surface concentrations of SO_4^{2-} and NO_3^- as discussed earlier but also those of OA and BC, with capturing only 8% (GIE and GIM) to 75%(SPR) of the observed OA values, and 8% (GIE and GIM) to 46% (SPR) of the observed BC values, respectively. At other stations in the IGP such as Agra, Allahabad and Hisar (Fig. 10), the surface concentrations of OA, BC, SO_4^{2-} and NO_3^- are underestimated in a similar degree by all models, although these stations are less populated than Kanpur. AOD and AAOD, indicating columnar aerosol loading, are also underestimated by all these models. It is well known that air pollutants are confined to near surface in winter due to the low ABL, thereby the results above suggest that the anthropogenic emissions used by the models (i.e., A2-ACCMIP and A2-MAP) are likely biased low. BC emissions in year 2000 over India from A2-ACCMIP and A2-MAP are 0.5Tg yr^{-1}, which is at the low end of a group of emission inventories, for instance, lower than those considered by REAS and GAINS-2008 emission inventories (Fig. 5a in Granier et al., 2011) by 40% or 0.3Tg yr^{-1}. With the REAS emission inventory, Nair et al. (2012) reported that the simulated BC surface concentration agreed better with observations at Kharagpur.

Different from other regions in northern hemisphere where fossil fuel burning and industrial processes tend to dominate, biofuel and open biomass burning in South Asia contribute two-

618 thirds of carbon-containing aerosols to form the dense brown clouds in winter (Gustafsson et
619 al., 2009). Over India, 42% of total BC emission is from biofuel, which is believed to be the
620 largest source of BC, with the remaining 33% from open biomass burning and 25% from fossil
621 fuel (Venkataraman et al., 2005). The percentage of biofuel is high because residential heating
622 and cooking (burning of wood, paper or other solid wastes) is quite common in South Asia,
623 especially among the underprivileged, leading to large amount of smoke comprised mainly of
624 black carbon and condensed semi-volatile organics. Based on in-situ measurements, the ratios
625 of OC/BC surface concentrations were reported as high as 8.0±2.2 at Allahabad (Ram et al.,
626 2012a) and 8.5±2.2 at Hisar (Rengarajan et al., 2007) in December 2004, indicating a major
627 emission source from biomass combustion including biofuel and open biomass burning
628 (Husain et al., 2007). However, in this study, fossil fuel are the dominant emission sources
629 instead, because the ratio of OC/BC anthropogenic emission (from combination of fossil fuel
630 and biofuel) in A2-ACMMIP (A2-MAP) emission database is 3.2 (2.6) (see Section 2.2) over
631 South Asia, and thus it is not surprising that the ratios of OC/BC surface concentrations are
632 found only varying 0.4-4.0 across models at Allahabad and 0.6-3.8 at Hisar. Although the ratio
633 of OC/BC in open biomass burning emission database is higher with a value of 8.0, open
634 biomass burning emissions are very low in winter, only 4% of anthropogenic emissions (see
635 Fig.2 and Fig.3). Furthermore, we found that the simulated BC surface concentrations by most
636 models agree better with the observations at Kharagpur than at other stations (Fig. 9). As
637 reported by Prasad et al. (2006), the sources of BC at Kharagpur located in eastern IGP were
638 mainly linked to the clusters of the coal-based industries there. Therefore, this contrast
639 suggests that the fossil fuel emissions are likely better represented than the biofuel emissions
640 in the A2-MAP and A2-ACCMIP emission inventories. In addition, the lack of seasonal
641 variation in anthropogenic emission datasets would amplify the underestimation of aerosol
642 amount during the winter when biofuel emissions are prevalent. In sum, the model
643 underestimation of anthropogenic OA and BC concentrations in winter is mostly due to the
644 underestimation of biofuel emissions.
645
646 **6.4 Agriculture waste burning emissions**
647 During the post-monsoon season (October-November), the extensive agriculture waste
648 burning after harvest in northwest India (e.g., Punjab) makes a large contribution to the dense
649 haze over South Asia based on previous observational studies (Vadrevu et al., 2011; Sharma
650 et al., 2010). The agricultural fires in this area are evident in the MODIS fire count product.
651 Smoke plumes from Punjab also impact the downwind regions by eastward transport along
652 IGP and southward to central-south India (Sharma et al., 2010; Badarinath et al., 2009a, b).
653 Over India, the contribution from open biomass burning to the total BC emission is
654 significant, about half of anthropogenic emissions (i.e. biofuel plus fossil fuel emissions)
655 (Venkataraman et al., 2005). The biomass burning contribution is evident based on the
656 AERONET data at Lahore, where AAOD enhances by 70% in November (after harvest) from
657 previous months (Fig. 5), and its contribution is also clearly seen in the MODIS-Terra and
658 Aqua data with the maximum AOD found near Lahore in the post-monsoon season (the fourth

column of Fig. 7a). BC emission from open biomass burning (based on GFED2) used by the models, however, is less than 1% of that from anthropogenic sources (comparing Fig. 2 and Fig. 3) during the post-monsoon season, both on regional average and in areas around Lahore, Therefore, it is not surprising that all models fail to capture high AAOD and AOD in this season (Fig. 5 and Fig. 7b). The underestimation of BC emission from agriculture waste burning also implies a similar degree of underestimation of OC from the same source.

The open biomass burning emission from GFED2 is derived from MODIS burned area products. It was previously reported that the small fires such as agricultural waste burning were largely missing in the GFED product (e.g. van der Werf et al., 2010; Randerson et al., 2012). The agricultural waste burning area is usually underestimated or overlooked in MODIS because the size of agriculture fires is too small to generate detectable burn scars in the 500 meter pixel resolution of MODIS product (van der Werf et al., 2010; Randerson et al., 2012).

6.5 Other factors

Other factors can also cause the models to underestimate AOD. For example, the observed ratio of secondary organic carbon (SOC) to primary OC is 30% - 40% in several stations located in North India, suggesting a significant contribution from SOC (Rengarajan et al., 2007; Ram and Sarin et al., 2010a). However, only two models include a resolved SOC chemistry. In addition, although the dust emission is minimal in winter compared to anthropogenic emission, dust sources from road traffic, soil re-suspension, and construction activity in the urban regions of the IGP (Tripathi et al., 2006; Tiwari et al., 2009) could be important, which are not considered in the current models.

Some difficulties with the models might be associated with the coarse spatial resolution (at 1.1° – 2.8°, see Table 1). Considering the complex terrain variations over South Asia, especially the valley-type topography of the IGP region with the towering Himalaya in the north (Fig. 1), the aerosol processes may not be adequately represented at such coarse spatial resolution. In addition, because of the non-linearity of wind-dependent dust emission and RH-dependent aerosol hygroscopic growth, a finer model spatial resolution would result in a higher dust emission and AOD (Bian et al., 2009).

Another important factor contributing to high surface aerosol concentrations in winter over South Asia is the shallow wintertime ABL that suppresses ventilation thereby trapping pollutants near the surface. At Kanpur, ABL height is about 200 m in winter according to the observations (Tripathi et al., 2006; Nair et al., 2007). However, the averaged ABL in GOC and GE5 models are 400-500 m in the study region (other models did not provide this information), allowing more efficient vertical mixing to dilute the surface concentrations and thus contributing to the low bias of surface aerosol concentration (Fig. 9 and 10). Therefore, a better-constrained ABL would be helpful to reduce the model bias of surface concentrations. Here we would like to iterate, however, that the columnar AOD and AAOD during wintertime is underestimated by the models as well, despite to a lesser degree than the underestimation of surface concentration (for example, model-simulated BC concentrations are too low by a factor of about 10, compared to the underestimation of AAOD by a factor of ~3). Considering the results that both aerosol surface concentration and columnar loading are underestimated, the

dominant factor in underestimating aerosol surface concentrations by these models is likely the underestimation of the emissions in wintertime, as addressed in Section 6.3.

7. Conclusions

In this study, the aerosol simulations for 2000-2007 from seven global aerosol models are evaluated with satellite data and ground-based measurements over South Asia, in particular over IGP, one of the heavily polluted regions in the world. The high AOD over IGP is associated with persistent high aerosol and precursor gas emissions (such as dust, SO_2, NO_x, NH_3, OA and BC) from local and upwind regions, and with its valley-type topography (bounded by the towering Himalaya) that is conducive to trapping both anthropogenic and dust aerosols in this region. The main results of this study are summarized below.

1. Averaged over the entire South Asia for 2000-2007, the annual mean AOD is about 0.27-0.33 from satellites retrievals. Six out of seven global models consistently underestimate the annual mean AOD by 15%-44% compared to MISR, the lowest bound of four satellite datasets used in the present study. The model performances are worse over northern India. In general, the underestimation of aerosol loading is mainly found during the winter and post-monsoon months when anthropogenic and open biomass burning emissions are dominant.
2. During wintertime (DJF), six out of seven models largely underestimate columnar AOD and AAOD over Indian subcontinent, and the underestimations of aerosol extinction generally occur in the lower troposphere (below 2 km). The simulated surface mass concentrations of SO_4^{2-}, NO_3^-, OA and BC are as small as 0.1-60% of the observed values in winter. Several possible causes for the common underestimations are identified: (a) the wintertime near-surface relative humidity is too low (e.g., about 20% in IGP in six out of seven models, compared to the observed value of > 60%) such that the hygroscopic growth of soluble aerosols and formation of secondary inorganic aerosol (NO_3^- and SO_4^{2-}) are suppressed; (b) NO_3^- is either missing or inadequately accounted for; (c) anthropogenic emission, especially from biofuel in winter, is underestimated in the emission datasets. The lack of seasonal variation of emissions amplifies the discrepancies in winter.
3. During the post-monsoon season (ON), none of the models capture the observed high AOD over western and central IGP. AAOD and BC surface concentrations are underestimated at the stations in IGP as well. Such discrepancy is attributed largely to the underestimation of open biomass burning in the satellite-based emission inventory (GFED2). It is likely due to missing small agricultural waste burning that is difficult to be retrieved by the satellite remote-sensors.
4. As for the inter-model diversity, the results show that the largest diversity occurs in the treatment of dry deposition, with diversity of dry deposition amount ranging from 41 to 46% for BC, OA, and SO_4^{2-}. In contrast, the diversity of wet deposition is smaller, from 15 to 22% across three species. For mineral dust, the emission itself has very large diversity among the models (about 124%), leading to a similar diversity of dry deposition (aerodynamic dry deposition + gravitational settling) as of 115%, although the diversity of dust AOD is much smaller at 22%.

To sum up, we have identified the major discrepancies of seven state-of-the-art global aerosol models in simulating aerosol loading over South Asia. Results from this study suggest directions to improve model simulations over this important region, including improving meteorological fields (particularly relative humidity), revising biofuel and agriculture fire emission inventories, and adding/improving NO_3^-. Currently, we are working on quantifying the factors that cause the model underestimation by ranking their importance via a series of model sensitivity experiments using the GEOS5 model. Our ongoing work includes adjusting the model spatial resolution, emission strength, and meteorological variables and adding nitrate, which will be presented in subsequent publications. Here, we also would like to suggest to establish more systematic measurements, especially long-term (at least one year-around) surface and vertical characterization of aerosol composition, precursor gases, optical properties, and meteorological fields (e.g. temperature, winds, and relative humidity), because they are essential for understanding the aerosol physical and chemical characterization.

Acknowledgement

We thank the ICARB, ISRO-GBP, and AERONET networks for making their data available. Site PIs and data managers of those networks are gratefully acknowledged. We also thank the Goddard Earth Science Data and Information Services Center for providing gridded satellite products of SeaWiFS, MISR, and MODIS through their Giovanni website, and the AeroCom data management for providing access to the global model output used in this study. Dr. Brigitte Koffi is appreciated for providing L3 CALIOP data. X. Pan is supported by an appointment to the NASA Postdoctoral Program at the GSFC, administered by Oak Ridge Associated Universities through a contract with NASA. The work by MC, HB, DK, and PC are supported by the NASA MAP and ACMAP Programs. SEB and KT have been supported by the NASA MAP program (NN-H-04-Z-YS-008-N and NN-H-08-Z-DA-001-N). L. Pozzoli was supported by PEGASOS (FP7-ENV-2010-265148). ECHAM5-HAMMOZ simulations were supported by the Deutsches Klimarechenzentrum (DKRZ) and the Forschungszentrum Juelich. Resources supporting this work were provided by the NASA High-End Computing (HEC) Program through the NASA Center for Climate Simulation (NCCS) at Goddard Space Flight Center. We are grateful to two reviewers for their constructive and helpful comments.

References

Ali, K., Momin, G.A., Tiwari, S., Safai, P.D., Chate, D.M., Rao, P.S.P.: Fog and precipitation chemistry at Delhi, North India. Atmos. Environ., 38, 4215–4222, 2004.

Badarinath, K.V.S., Kharol, S.K. and Sharma, A. R.: Long-range transport of aerosols from agriculture crop residue burning in Indo-Gangetic Plains—A study using LIDAR, ground measurements and satellite data, J. Atmos. Sol. Terr. Phys., 71, 112– 120, doi:10.1016/j.jastp.2008.09.035, 2009a.

Badarinath, K.V.S., Kharol,S.K., Sharma, A.R., V. Krishna Prasad: Analysis of aerosol and carbon monoxide characteristics over Arabian Sea during crop residue burning period in the Indo-Gangetic Plains using multi-satellite remote sensing datasets, J. Atmos. Solar-Terr. Phys., 71, 1267 – 1276, 2009b.

Babu, S. S., Manoj, M. R., Moorthy, K. K., Gogoi, M. M., Nair, V. S., Kumar Kompalli, S.,

790 Satheesh, S. K., Niranjan, K., Ramagopal, K., Bhuyan, P. K., and Singh, D.: Trends in aerosol
791 optical depth over Indian region: potential causes and impact indicators, J. Geophys. Res.Atmos.,
792 118, 11794–11806, doi:10.1002/2013JD020507, 2013.
793
794 Bauer, S.E., Wright, D., Koch, D., Lewis, E.R., McGraw, R., Chang, L.-S. Schwartz, S.E. and
795 Ruedy, R.: MATRIX (Multiconfiguration Aerosol TRacker of mIXing state): An aerosol
796 microphysical module for global atmospheric models. Atmos. Chem. Phys., 8, 6603-6035,
797 doi:10.5194/acp-8-6003-2008, 2008.
798
799 Bauer, S.E., Menon, S., Koch, D., Bond, T.C., and Tsigaridis, K.: A global modeling study on
800 carbonaceous aerosol microphysical characteristics and radiative forcing. Atmos. Chem. Phys., 10,
801 7439-7456, doi:10.5194/acp-10-7439-2010, 2010.
802
803 Beegum, S., Moorthy, S.N., Babu, K.K.,Satheesh, S.S., Vinoj,S.K., Badarinath,V., Safai,
804 K.V.S., Devara, P.D., Singh, P.C.S., Vinod, S., Dumka U. C., Pant, P.: Spatial distribution of
805 aerosol black carbon over India during pre-monsoon season. Atmos. Environ. 43, 071e1078, 2009.
806
807 Bellouin, N., Rae, J., Jones, A., Johnson, C., Haywood, J. and Boucher, O.: Aerosol forcing in the
808 Climate Model Intercomparison Project (CMIP5) simulations by HadGEM2□ES and the role of
809 ammonium nitrate, J. Geophys. Res., 116, D20206, doi:10.1029/2011JD016074, 2011.
810
811 Bian, H., Chin, M., Rodriguez, J., Yu, H.,Penner, J. E., Strahan, S.: Sensitivity of aerosol optical
812 thickness and aerosol direct radiative effect to relative humidity, Atmos. Chem. Phys., 9, 2375-
813 2386, 2009.
814
815 Bond, T. C., and Bergstrom, R. W.: Light absorption by carbonaceous particles: An investigative
816 review, Aerosol Sci. Technol., 40(1), 27–67, doi:10.1080/02786820500421521, 2006.
817
818 Bond, TDoherty, S. J., Fahey, D. W., Forster, P. M., Berntsen, T., DeAngelo, B. J., Flanner, M.
819 Ghan, K¨archer, B., Koch, D., Kinne,Kondo, Y., Quinn, P. Sarofim, M. C., Schultz, MSchulz, M.,
820 Venkataraman, C., Zhang, H., Zhang, S., Bellouin, N., Guttikunda, S. Hopke, P. K., Jacobson, M.
821 Z., Kaiser, J. W., Klimont, Z., Lohmann, U., Schwarz, J. P., Shindell, D., Storelvmo, T., Warren, S.
822 G., and Zender, C. S.: Bounding the role of black carbon in the climate system: A scientific
823 assessment, J.Res., 118, 5380–5552, doi:10.1002/jgrd.50171, 2013.
824
825 CALIPSO: CALIPSO Quality Statements Lidar Level 3 Aerosol Profile Monthly Products Version
826 Release: 1.00, 2011.
827
828 Cherian, R., Venkataraman, C., Quaas, J. and Ramachandran, S.: GCM simulations of
829 anthropogenic aerosol-induced changes in aerosol extinction, atmospheric heating and
830 precipitation over India, J. Geophys. Res. Atmos.,118, 2938–2955, doi:10.1002/jgrd.50298, 2013.
831
832 Chin, M., Ginoux, P., Kinne, S., Torres, O., Holben, B. N., Duncan, B. N., Martin, R. V., Logan, J.
833 A., Higurashi, A. and Nakajima, T.: Tropospheric aerosol optical thickness from the GOCART
834 model and comparisons with satellite and sun photometer measurements, J. Atmos., Sci., 59, 461-
835 483, 2002.
836
837 Chin, M., Diehl, T., Dubovik, O., Eck, T. F., Holben, B. N., Sinyuk, A. and Streets, D. G. : Light
838 absorption by pollution, dust and biomass burning aerosols: A global model study and evaluation
839 with AERONET data, Ann. Geophys., 27, 3439- 3464, 2009.

Chin, M., Diehl, T., Tan, Q., Prospero, J. M., Kahn, R. A., Remer, L. A., Yu, H., Sayer, A. M., Bian, H., Geogdzhayev, I. V., Holben, B. N., Howell, S. G., Huebert, B. J., Hsu, N. C., Kim, D., Kucsera, T. L., Levy, R. C., Mishchenko, M. I., Pan, X., Quinn, P. K., Schuster, G. L., Streets, D. G., Strode, S. A., Torres, O., and Zhao, X.-P.: Multi-decadal aerosol variations from 1980 to 2009: a perspective from observations and a global model, Atmos. Chem. Phys., 14, 3657-3690, doi:10.5194/acp-14-3657-2014, 2014.

Colarco, P. R., da Silva, A., Chin, M., and Diehl, T.: Online simulations of global aerosol distributions in the NASA GEOS-4 model and comparisons to satellite and ground-based aerosol optical depth, J. Geophys. Res., 115, D14207, doi:10.1029/2009JD012820, 2010.

Das, S. K., Jayaraman, A., and Misra, A.: Fog-induced variations in aerosol optical and physical properties over the Indo-Gangetic Basin and impact to aerosol radiative forcing, Ann. Geophys., 26, 1345-1354, doi:10.5194/angeo-26-1345-2008, 2008.

Diehl, T., Heil, A., Chin, M., Pan, X., Streets, D., Schultz, M., and Kinne, S.: Anthropogenic, biomass burning, and volcanic emissions of black carbon, organic carbon, and SO_2 from 1980 to 2010 for hindcast model experiments, Atmos. Chem. Phys. Discuss., 12, 24895-24954, 2012.

Feng, Y. and Penner, J. E.: Global modeling of nitrate and ammonium: Interaction of aerosols and tropospheric chemistry, J. Geophys. Res., Vol. 112, D01304, doi: 10.1029/2005JD006404, 2007.

Ganguly, D., Jayaraman, A., Rajesh, T. A. and Gadhavi, H.: Wintertime aerosol properties during foggy and nonfoggy days over urban center Delhi and their implications for shortwave radiative forcing, J. Geophys. Res., 111, D15217, doi:10.1029/2005JD007029, 2006.

Ganguly, D., Ginoux, P., Ramaswamy, V., Winker, D. M., Holben, B. N. and Tripathi, S. N.: Retrieving the composition and concentration of aerosols over the Indo-Gangetic basin using CALIOP and AERONET data, Geophys. Res. Lett., 36, L13806, doi:10.1029/2009GL038315, 2009.

Gautam, R., Hsu, N. C., Kafatos, M. and Tsay, S.-C.: Influences of winter haze on fog/low cloud over the Indo-Gangetic Plains, J. Geophys. Res., 112, D05207, doi:10.1029/2005JD007036, 2007.

Gautam R., Hsu, N. C., Lau, W. K.-M. and Yasunari, T. J.: Satellite observations of desert dust-induced Himalayan snow darkening, Geophys. Res. Lett., 40, 988–993, doi:10.1002/grl.50226, 2013.

Girolamo, D. L., Bond, T. C., Bramer, D., Diner, D. J., Fettinger, F. , Kahn, R. A. Martonchik, J. V. , Ramana, M. V., Ramanathan, V. and Rasch, P. J.: Analysis of Multi-angle Imaging SpectroRadiometer (MISR) aerosol optical depths over greater India during winter 2001–2004, Geophys. Res. Lett., 31, L23115, doi:10.1029/ 2004GL021273, 2004.

Goto, D., Takemura, T., Nakajima, T. and Badarinath, K. V. S.: Global aerosol model-derived black carbon concentration and single scattering albedo over Indian region and its comparison with ground observations, Atmos. Environ., 45(19), 3277–3285, 2011.

Granier, C., Bessagnet, B., Bond, T., D'Angiola, A., van der Gon, H. D., Frost, G. J., Heil, A., Kaiser, J. W., Kinne, S., Klimont, Z., Kloster, S., Lamarque, J.-F., Liousse, C., Masui, T., Meleux, F., Mieville, A., Ohara, T., Raut, J. C., Riahi, K., Schultz, M. G., Smith, S. J., Thompson, A., van

Aardenne, J., van der Werf, G. R., and van Vuuren, D. P.: Evolution of anthropogenic and biomass burning emissions of air pollutants at global and regional scales during the 1980–2010 period, Climatic Change, 109, 163–190, doi:10.1007/s10584-011-0154-1, 2011.

Gustafsson, O., Krusa, M., Zencak, Z., Sheesley, R. J., Granat, L., Engstrom, E., Praveen, P. S., Rao, P. S. P., Leck, C., and Rodhe, H.: Brown Clouds over South Asia: Biomass or Fossil Fuel Combustion?, Science, 323, 495–498, 2009.

Henriksson, S. V., Laaksonen, A., Kerminen, V.-M., Räisänen, P., Järvinen, H., Sundström, A.-M., and de Leeuw, G.: Spatial distributions and seasonal cycles of aerosols in India and China seen in global climate-aerosol model, Atmos. Chem. Phys., 11, 7975-7990, doi:10.5194/acp-11-7975-2011, 2011.

Hess, M., K¨opke, P., and Schult, I.: Optical properties of aerosols and clouds: The software package OPAC, B. Am. Meteorol. Assoc., 79, 831–844, doi: http://dx.doi.org/10.1175/1520-0477(1998)079<0831:OPOAAC>2.0.CO;2, 1998.

Holben, B.N., Eck, T.F., Slutsker, I., Tanre, D., Buis, J.P., Setzer, A., Vermote, E., Reagan, J.A., Kaufman, Y.J., Nakajima, T., Lavenu, F., Jankowiak, I., Smirnov, A.: AERONET — a federated instrument network and data archive for aerosol characterization. Remote Sens. Environ. 66, 1–16, 1998.

Hsu, N. C., Tsay, S.-C., King, M. D., and Herman, J. R.: Deep Blue retrievals of Asian aerosol properties during ACE-Asia, IEEE T. Geosci. Remote Sens., 44, 3180–3195, 2006.

Hsu, N. C., Gautam, R., Sayer, A. M., Bettenhausen, C., Li, C., Jeong, M. J., Tsay, S.-C., and Holben, B. N.: Global and regional trends of aerosol optical depth over land and ocean using SeaWiFS measurements from 1997 to 2010, Atmos. Chem. Phys., 12, 8037–8053, doi:10.5194/acp-12-8037-2012, 2012.

Husain, L., Dutkiewicz, V. A., Khan, A. J., Chin, M., and Ghauri, B. M.: Characterization of carbonaceous aerosols in urban air, Atmos. Envrion., 41, 6872–6883, 2007.

Jethva, H., Satheesh, S. K., Srinivasan, J., and Krishnamoorthy, K.: How Good is the Assumption about Visible Surface Reflectance in MODIS Aerosol Retrieval over Land? A Comparison with Aircraft Measurements over an Urban Site in India, IEEE Transactions on Geoscience and Remote Sensing, 47(7), 2009.

Kahn, R. A., W.-H. Li, C. Moroney, D. J. Diner, J. V. Martonchik, and E. Fishbein: Aerosol source plume physical characteristics from space-based multiangle imaging, J. Geophys. Res., 112, D11205, doi:10.1029/2006JD007647, 2007.

Kahn, R. A., Gaitley, B. J., Garay, M. J., Diner, D. J., Eck, T., Smirnov, A., and Holben, B. N.: Multiangle Imaging SpectroRadiometer global aerosol product assessment by comparison with the Aerosol Robotic Network, J. Geophys. Res., 115, D23209, doi:10.1029/2010JD014601, 2010.

Kaskaoutis, D. G., Singh, R. P., Gautam, R., Sharma, M., Kosmopoulos, P. G., Tripathi, S. N.: Variability and Trends of Aerosol Properties over Kanpur, Northern India Using AERONET Data (2001–10). Environ. Res. Lett.7: 024003, doi: 10.1088/1748-9326/7/2/024003, 2012.

Koffi, B., Schulz, M., Bréon, F.-M., Griesfeller, J., Winker, D., Balkanski, Y., Bauer, S., Berntsen,T., Chin, M., Collins, W. D., Dentener, F., Diehl, T., Easter, R., Ghan, S., Ginoux, P., Gong, S., Horowitz, L. W., Iversen, T., Kirkevåg, A., Koch, D., Krol, M., Myhre, G., Stier, P., and Takemura, T.: Application of the CALIOP layer product to evaluate the vertical distribution of aerosols estimated by global models: AeroCom phase I results, J. Geophys. Res.,117, D10201, doi:10.1029/2011JD016858, 2012.

Lau, K. M., Kim, M. K. and Kim, K. M.: Asian summer monsoon anomalies induced by aerosol direct forcing: The role of the Tibetan Plateau, Clim. Dyn., 26, 855–864, 2006.

Lau, K. M., Kim, M. K., Kim, K. M. and Lee, W. S.: Enhanced surface warming and accelerated snow melt in the Himalayas and Tibetan Plateau induced by absorbing aerosols, Env. Res. Lett., 5, 025204, doi:10.1088/1748-9326/5/2/025204, 2010.

Lawrence, M. G., and Lelieveld, J.: Atmospheric pollutant outflow from southern Asia: A review, Atmos. Chem. Phys., 10, 11,017–11,096, 2010.

Levy, R. C., Remer, L. A., Mattoo, S., Vermote, E. F., and Kaufman, Y. J.: Second-generation operational algorithm: Retrieval of aerosol properties over land from inversion of Moderate Resolution Imaging Spectroradiometer spectral reflectance, J. Geophys. Res., 112, D13211, doi:10.1029/2006JD007811, 2007.

Levy, R. C., Remer, L. A., Kleidman, R. G., Mattoo, S., Ichoku, C., Kahn, R., and Eck, T. F.: Global evaluation of the Collection 5 MODIS dark-target aerosol products over land, Atmos. Chem. Phys., 10, 10399–10420, doi:10.5194/acp-10-10399-2010, 2010.

Martonchik, J. V., Diner, D. J., Kahn, R., Gaitley, B. and Holben, B. N.: Comparison of MISR and AERONET aerosol optical depths over desert sites, Geophys. Res. Lett., 31, L16102, doi:10.1029/2004GL019807, 2004.

Menon, S., Koch, D., Beig, G., Sahu, S., Fasullo, J., and Orlikowski, D.: Black carbon aerosols and the third polar ice cap, Atmos. Chem. Phys., 10, 4559-4571, doi:10.5194/acp-10-4559-2010, 2010.

Moorthy, K. K., Beegum, S. N., Srivastava, N., Satheesh, S. K., Chin, M., Blond, N., Babu, S. S. and Singh, S.: Performance Evaluation of Chemistry Transport Models over India, Atmos. Environ., 71, 210–225, 2013.

Myhre, G., Samset, B. H., Schulz, M., Balkanski, Y., Bauer, S., Berntsen, T. K., Bian, H., Bellouin, N., Chin, M., Diehl, T., Easter, R. C., Feichter, J., Ghan, S. J., Hauglustaine, D., Iversen, T., Kinne, S., Kirkevåg, A., Lamarque, J.-F., Lin, G., Liu, X., Lund, M. T., Luo, G., Ma, X., van Noije, T., Penner, J. E., Rasch, P. J., Ruiz, A., Seland, Ø., Skeie, R. B., Stier, P., Takemura, T., Tsigaridis, K., Wang, P., Wang, Z., Xu, L., Yu, H., Yu, F., Yoon, J.-H., Zhang, K., Zhang, H., and Zhou, C.: Radiative forcing of the direct aerosol effect from AeroCom Phase II simulations, Atmos. Chem. Phys., 13, 1853-1877, doi:10.5194/acp-13-1853-2013, 2013.

Nair, V. S., Moorthy, K. K., Alappattu, D. P., Kunhikrishnan, P. K.,George, S., Nair, P. R., Babu, S. S., Abish, B., Satheesh, S. K., Tripathi, S. N., Niranjan, K., Madhavan, B. L., Srikant, V., Dutt, C. B. S., Badarinath, K. V. S., and Reddy, R. R.: Wintertime aerosol characteristics over the Indo-Gangetic Plain (IGP): Impacts of local boundary layer processes and long-range transport, J. Geophys. Res., 112, D13205, doi:10.1029/2006JD008099, 2007.

993 Nair, V. S., Solmon, F., Giorgi, F., Mariotti, L., Babu, S. S., and Moorthy, K. K.: Simulation of South
994 Asian aerosols for regional climate studies, J. Geophys. Res., 117, D04209,
995 doi:10.1029/2011JD016711, 2012.
996
997 Ohara, T., Akimoto, H., Kurokawa, J., Horii, N.,Yamaji, K., Yan, X. and Hayasaka, T. : An Asian
998 emission inventory of anthropogenic emission sources for the period 1980–2020, Atmos. Chem.
999 Phys., 7, 4419–4444, 2007.
000
001 Pozzoli, L., Janssens-Maenhout, G., Diehl, T., Bey, I., Schultz, M. G., Feichter, J., Vignati, E., and
002 Dentener, F.: Reanalysis of tropospheric sulphate aerosol and ozone for the period 1980–2005
003 using the aerosol-chemistry-climate model ECHAM5-HAMMOZ, Atmos. Chem. Phys. Discuss., 11,
004 10191-10263, doi:10.5194/acpd-11-10191-2011, 2011.
005
006 Prasad, A. K., Singh, R. P., and Kafatos, M.: Influence of coal based thermal power plants on
007 aerosol optical properties in the Indo-Gangetic basin, Geophys. Res. Lett., 33, L05805,
008 doi:10.1029/2005GL023801, 2006.
009
010 Qian, Y., Flanner, M. G., Leung, L. R. , and Wang W.: Sensitivity studies on the impacts of Tibetan
011 Plateau snowpack pollution on the Asian hydrological cycle and monsoon climate, Atmos. Chem.
012 Phys., 11, 1929–48, doi:10.5194/acp-11-1929-2011, 2011.
013
014 Ram K., Sarin, M. M.: Spatio-temporal variability in atmospheric abundances of EC, OC and
015 WSOC over Northern India, Journal of Aerosol Science, 41(1), 88-98, 2010a.
016
017 Ram, K., Sarin, M. M., and Tripathi, S. N.: A 1 year record of carbonaceous aerosols from an urban
018 site in the Indo-Gangetic Plain: Characterization, sources, and temporal variability, J. Geophys.
019 Res., 115, D24313, doi:10.1029/2010JD014188, 2010b.
020
021 Ram, K., Sarin, M. M., Sudheer, A. K. and Rengarajan, R.: Carbonaceous and secondary inorganic
022 aerosols during wintertime fog and haze over urban sites in the Indo-Gangetic Plain, Aerosol Air
023 Qual.Res.,12,359–370, 2012a.
024
025 Ram, K., Sarin, M.M., Tripathi, S.N.: Temporal trends in atmospheric PM2.5, PM10, elemental
026 carbon, organic carbon, water-soluble organic carbon, and optical properties: impact of biomass
027 burning emissions in the Indo-Gangetic Plain. Environmental Science & Technology 46, 686-695,
028 2012b.
029
030 Ramachandran, S., Rengarajan, R., Jayaraman, A., Sarin, M. M. and Das, S. K.: Aerosol radiative
031 forcing during clear, hazy, and foggy conditions over a continental polluted location in north India, J.
032 Geophys. Res., 111, D20214, doi:10.1029/2006JD007142, 2006.
033
034 Ramachandran, S., and Kedia S.: Aerosol, clouds and rainfall: inter-annual and regional variations
035 over India, Clim. Dyn., 40(7–8), 1591–1610, doi:10.1007/s00382-012-1594-7, 2013.
036
037 Ramanathan, V., Crutzen, P. J., Lelieveld, J., Mitra, A. P., Althausen, D., Anderson, J., Andreae, M.
038 O., Cantrell, W., Cass, G. R., Chung, C. E., Clarke, A. D., Coakley, J. A., Collins,W. D., Conant, W.
039 C., Dulac, F., Heintzenberg, J., Heymsfield, A. J., Holben, B., Howell, S., Hudson, J., Jayaraman,
040 A., Kiehl, J. T., Krishnamurti, T. N., Lubin, D., McFarquhar, G., Novakov, T., Ogren, J. A.,
041 Podgorny, I. A., Prather, K., Priestley, K., Prospero, J. M., Quinn, P. K., Rajeev, K., Rasch, P.,
042 Rupert, S., Sadourny, R., Satheesh, S. K., Shaw, G. E., Sheridan, P., and Valero, F. P. J.: Indian

043 Ocean Experiment: An integrated analysis of the climate forcing and effects of the great Indio-
044 Asian haze, J. Geophys. Res., 106, 28371–28398, 2001.
045
046 Ramanathan V., Chung C., Kim D., Bettge T., Buja L., Kiehl J.T., Washington W.M., Fu Q., Sikka
047 D.R., Wild M..: Atmospheric brown clouds: impact on South Asian climate and hydrologic cycle.
048 Proc Natl Acad Sci 102:5326–5333, DOI 10.1073/pnas.0500656102, 2005.
049
050 Randerson, J. T., Chen, Y., van der Werf, G. R., Rogers, B. M., and Morton, D. C.: Global burned
051 area and biomass burning emissions from small fires, J. Geophys. Res., 117, G04012,
052 doi:10.1029/2012JG002128, 2012.
053
054 Reddy, M. S., Boucher, O., Venkataraman, C., Verma, S., Le´on, J.-F., Bellouin, N., and Pham, M.:
055 General circulation model estimates of aerosol transport and radiative forcing during the Indian
056 Ocean Experiment, J. Geophys. Res., 109, D16205, doi:10.1029/2004JD004557, 2004.
057
058 Rengarajan, R., Sarin, M. M., and Sudheer, A. K.: Carbonaceous and inorganic species in
059 atmospheric aerosols during wintertime over urban and high-altitude sites in North India, J.
060 Geophys. Res., 112, D21307, doi:10.1029/2006JD008150, 2007.
061
062 Safai, P. D., Kewat, S. , Pandithurai, G., Praveen, P. S., Ali, K., Tiwari, S., Rao, P. S. P.,
063 Budhawant, K. B., Saha, S. K., Devara, P. C. S.: Aerosol characteristics during winter fog at Agra,
064 North India. J. Atmos. Chem., 61(2), 101–118, 2008.
065
066 Sahu, S. K., Beig. G., and Sharma, C.: Decadal growth of black carbon emissions in India,
067 Geophys. Res. Lett., 35, L02807, doi:10.1029/ 2007GL032333, 2008.
068
069 Sanap, S.D., Ayantika, D.C., Pandithurai, G., Niranjan, K.: Assessment of the aerosol distribution
070 over Indian subcontinent in CMIP5 models, Atmospheric Environment, 87,123-137, 2014.
071
072 Sayer, A. M., Hsu, N. C., Bettenhausen, C., Ahmad, Z., Holben, B. N., Smirnov, A., Thomas, G. E.,
073 and Zhang, J.: SeaWiFS Ocean Aerosol Retrieval (SOAR): algorithm, validation, and comparison
074 with other datasets, J. Geophs. Res, 117, D03206,doi:10.1029/2011JD016599, 2012.
075
076 Sayer, A. M., Hsu, N. C., Bettenhausen, C., and Jeong, M.-J.: Validation and uncertainty estimates
077 for MODIS Collection 6 “Deep Blue” aerosol data, J. Geophys. Res. Atmos., 118,7864–7872,
078 doi:10.1002/jgrd.50600, 2013.
079
080 Sessions, W. R., Reid, J. S., Benedetti, A., Colarco, P. R., da Silva, A., Lu, S., Sekiyama, T.,
081 Tanaka, T. Y., Baldasano, J. M., Basart, S., Brooks, M. E., Eck, T. F., Iredell, M., Hansen, J. A.,
082 Jorba, O. C., Juang, H.-M. H., Lynch, P., Morcrette, J.-J., Moorthi, S., Mulcahy, J., Pradhan, Y.,
083 Razinger, M., Sampson, C. B., Wang, J., and Westphal, D. L.: Development towards a global
084 operational aerosol consensus: basic climatological characteristics of the International Cooperative
085 for Aerosol Prediction Multi-Model Ensemble (ICAP-MME), Atmos. Chem. Phys., 15, 335-362,
086 doi:10.5194/acp-15-335-2015, 2015.
087
088 Sharma, A.R., Kharol, S.K., Badarinath, K.V.S., Singh, D.: Impact of agriculture crop residue
089 burning on atmospheric aerosol loading — a study over Punjab State, India. Ann. Geophys. 28,
090 367–379, 2010.
091
092 Singh T., Khillare P.S., Shridhar V., Agarwal T.: Visibility impairing aerosols in the urban
093 atmosphere of Delhi. Environ Monit Assess 141:67–77, 2008.

094
095 Srivastava, A. K., Tripathi, S. N., Dey, S., Kanawade, V. P., and Tiwari, S.: Inferring aerosol types
096 over the Indo-Gangetic Basin from ground based sunphotometer measurements, Atmos. Res.,
097 109–110, 64–75, doi:10.1016/j.atmosres.2012.02.010, 2012a.
098
099 Srivastava, A.K., Singh, S., Pant, P., Dumka, U.C.: Characteristics of black carbon over Delhi and
100 Manora Peak-a comparative study. Atmos Sci Lett 13:223–230. doi:10.1002/asl.386, 2012b.
101
102 Takemura, T., Nozawa, T., Emori, S., Nakajima, T. Y., and Nakajima,T.: Simulation of climate
103 response to aerosol direct and indirect effects with aerosol transport-radiation model, J.
104 Geophys.Res.-Atmos., 110, D02202, doi:10.1029/2004jd005029, 2005.
105
106 Takemura, T., Egashira, M., Matsuzawa, K., Ichijo, H., O'Ishi, R., and Abe-Ouchi, A.: A simulation
107 of the global distribution and radiative forcing of soil dust aerosols at the Last Glacial Maximum,
108 Atmos. Chem. Phys., 9, 3061–3073, doi:10.5194/acp-9-3061-2009, 2009.
109
110 Tare, V., Tripathi, S.N., Chinnam, N., Srivastava, A.K., Dey, S., Manar, M., Kanawade, V.P.,
111 Agarwal, A., Kishore, S., Lal, R.B., Sharma, M.: Measurements of atmospheric parameters during
112 Indian Space Research Organization Geosphere Biosphere Program Land Campaign II at a typical
113 location in the Ganga Basin: 2. Chemical properties, J. Geophys. Res., 111, D23210,
114 doi:10.1029/2006JD007279, 2006.
115
116 Textor, Schulz, M., Guibert, S., Kinne, Balkanski, Bauer, S., Berntsen, T., Berglen, T., Boucher, O.,
117 Chin, M., Dentener, Diehl, T., Feichter, Fillmore, D., Ginoux, Gong, S., Grini, Hendricks, J.,
118 Horowitz, L., Huang, P., Isaksen, I. S. A., Iversen, T., Kloster, S., Koch, D.,
119 Kirkevåg, Kristjansson, J. E., Krol, M., Lauer, A., Lamarque, J. F., Liu, X., Montanaro, V., Myhre, G.,
120 Penner, J. E., Pitari, G., Reddy, M. S., Seland, Ø., Stier, P., Takemura, T., and Tie, X.: The effect
121 of harmonized emissions on aerosol properties in global models – an AeroCom experiment, Atmos.
122 7, 4489-4501, doi:10.5194/acp-7-4489-2007, 2007.
123
124 Tiwari, S., Srivastava,A.K.,Bisht,D.S., Bano, T., Singh, S.,Behura, S., Srivastava,M.K.,Chate, D.M.,
125 Padmanabhamurty, B.: Black carbon and chemical characteristics of PM10 and PM2.5 at an urban
126 site of North India. J. Atmos. Chem. 62(3), 193–209. doi:10.1007/s10874-010-9148-z, 2009.
127
128 Tripathi, S. N., Tare, V., Chinnam, N., Srivastava, A. K., Dey, S., Agarwal, A., Kishore, S., Lal, R.
129 B., Manar, M., Kanwade, V. P., Chauhan, S. S. S., Sharma, M., Reddy, R. R., Gopal, K. R.,
130 Narasimhulu, K., Reddy, L. S. S., Gupta, S., and Lal, S.:
131 Measurements of atmospheric parameters during Indian Space Research Organization Geosphere
132 Biosphere Programme Land Campaign II at a typical location in the Ganga basin: 1. Physical and
133 optical properties, J. Geophys. Res., 111, D23209, doi:10.1029/2006JD007278, 2006.
134
135 Tsigaridis, K., Koch, D. M., and Menon, S.: Uncertainties and importance of sea-spray composition
136 on aerosol direct and indirect effects, J. Geophys. Res., 118, 220–235, doi:10.1029/2012JD018165,
137 2013.
138
139 Vadrevu, K.P., Ellicott, E., Badarinath, K.V.S., Vermote, E.: MODIS derived fire characteristics and
140 aerosol optical depth variations during the agricultural residue burning season, north India.
141 Environmental Pollution 159, 1560-1569, 2011.
142
143 Vadrevu, K. P., Giglio, L., Justice C.: Satellite based analysis of fire–carbon monoxide relationships
144 from forest and agricultural residue burning (2003–2011), Atmos. Environ., 64,179-191, 2013.

van der Werf, G. R., Randerson, J. T., Giglio, L., Collatz, G. J., Mu, M., Kasibhatla, P. S., Morton, D. C., DeFries, R. S., Jin, Y., and van Leeuwen, T. T.: Global fire emissions and the contribution of deforestation, savanna, forest, agricultural, and peat fires (1997–2009), Atmos. Chem. Phys., 10, 11707–11735, doi:10.5194/acp-10-11707-2010, 2010.

Venkataraman, C., Habib, G., Eiguren-Fernandez, A., Miguel, A. H., and Friedlander, S. K.: Residential biofuels in south asia: Carbonaceous aerosol emissions and climate impacts, Science, 307, 1454–1456, 2005.

Venkataraman, C., Habib, G., Kadamba, D., Shrivastava, M., Leon, J.-F., Crouzille, B., Boucher, O. and Streets, D. G.: Emissions from open biomass burning in India: Integrating the inventory approach with high-resolution Moderate Resolution Imaging Spectroradiometer (MODIS) active-fire and land cover data, Global Biogeochem. Cycles, 20, GB2013, doi:10.1029/2005GB002547, 2006.

Yasunari, T. J., Bonasoni, P., Laj, P., Fujita, K., Vuillermoz, E., Marinoni, A., Cristofanelli, P., Duchi, R., Tartari, G., and Lau, K.-M.: Estimated impact of black carbon deposition during pre-monsoon season from Nepal Climate Observatory – Pyramid data and snow albedo changes over Himalayan glaciers, Atmos. Chem. Phys., 10, 6603-6615, doi:10.5194/acp-10-6603-2010, 2010.

Yu, F., Luo, G., and Ma, X.: Regional and global modeling of aerosol optical properties with a size, composition, and mixing state resolved particle microphysics model, Atmos. Chem. Phys., 12, 5719-5736, doi:10.5194/acp-12-5719-2012, 2012.

Tables

Table1. General information of models used in this study.

Model		HadGEM2	GOCART-v4	ECHAM5-HAMMOZ	GISS-modelE	GISS-MATRIX	SPRIN-TARS	GEOS5-GOCART
ID		HAD	GOC	ECH	GIE	GIM	SPR	GE5
Time range		2000-2006	2000-2007	2000-2005	2000-2008	2000-2007	2000-2008	2000-2008
Spatial Resolution [a]		1.8×1.2×38	2.5×2×30	2.8×2.8×31	2.5×2×40	2.5×2×40	1.1×1.1×56	2.5×2×72
Anthrp. Emi. [b]		A2-MAP	A2-MAP	A2-MAP	A2-ACCMIP	A2-ACCMIP	A2-ACCMIP	A2-ACCMIP
BB Emi. [c]		GFED2	GFED2	GFED2	GFED2	GFED2	GFED2	GFED2
Met. Field		ERA- Interim	GEOS-DAS	ECMWF analysis	NCEP wind	NCEP-wind	NCEP/ NCAR	MERRA
Refrac-tive index 550nm	SO_4^{2-}	1.53 – 1e-7*i*	1.43-1e-8 *i*	1.43-1e-8*i* [e]	1.528-1e-7*i*	1.528-1e-7*i*	1.43-1e-8*i*	1.43-1e-8*i*
	BC	1.75 – 0.44*i* (FF) [d]	1.75-0.44*i*	1.85-0.71*i*	1.85-0.71*i*	1.85-0.71*i*	1.75-0.44*i*	1.75-0.44*i*
	OA	1.54 – 0.006*i* (FF)	1.53-0.006*i*	1.53-0.0055*i*	1.527-0.014*i*	1.527-0.014*i*	1.53-0.006*i*	1.53-0.006*i*
	Dust	1.52 – 0.0015*i*	1.53-0.0055*i*	1.517-0.0011*i*	1.564-0.002*i*	1.564-0.002*i*	1.53-0.002*i*	1.53-0.008i
	SS	1.55 – 1e-7*i* Aged BB: 1.54 – 0.018*i*	1.50-1e-8 *i*	1.49-1e-8*i*	1.45-0.*i*	1.45-0.*i*	1.38-4.26e-9*i*	1.50- 1e-8*i*
Additional Species [f]		NO_3^-	-	-	NO_3^-	NO_3^-	-	-
Dust Size distribution (μm) [g]		6 bins 0.0316-0.1-0.316-1.0-3.16-10-31.6	8 bins 0.1-0.18-0.3-0.6-1.0-1.8-3.0-6.0-10.0	Accum. mode: 0.05<r_m<0.5 coarse mode: r_m>0.5	5 bins 0.1-1-2-4-8-16	4 bins 0-1-2-4-8	6 bins 0.1-0.22-0.46-1.0-2.15-4.64-10.0	8 bins 0.1-0.18-0.3-0.6-1.0-1.8-3.0-6.0-10.0
References		Bellouin et al., 2011	Chin et al., 2002, 2014	Pozzoli et al., 2011	Tsigaridis et al., 2013	Bauer et al., 2008, 2010	Takemura et al., 2005, 2009	Colarco et al., 2010

[a] Spatial resolutions (°latitude × °longitude × number of vertical levels).
[b] Anthropogenic emission data are from either A2-ACCMIP or A2-MAP (refer to Diehl et al. 2012).
[c] Biomass burning emission data (refer to Diehl et al. 2012).
[d] FF is fossil fuel and BB is biomass burning.
[e] As for EHCAM5-HAMMOZ model with a mixed aerosol scheme, the refractive index for each of the 7 modes is calculated as the volume weighted average of the refractive indices of the components of the mode, including the diagnosed aerosol water.
[f] Additional aerosols besides commonly included aerosol species, i.e. SO_4^{2-} (sulfate), Dust, SS (sea salt), BC (black carbon), and OA (organic aerosol). Here NO_3^- is nitrate.
[g] Listed is the edges of size bins in all models except for ECH, in which r_m is modal radii.

Table 2. Summary of stations in South Asia used in this study

Type	Station [a]	Lat	Lon	Alt (*m*)	Popul-ation [b] (*milli-*)	Data Source [c]	Data Category	Main Feature
Urban	Delhi	28.58º N	77.20º E	260	16.75	ICARB	BC	In western IGP, the largest city in India
	Karachi	24.87º N	67.03º E	49	13	AERONET	AOD AAOD	Coastal location in southern Pakistan
	Lahore	31.54º N	74.32º E	270	9	AERONET	AOD AAOD	In western IGP, major agricultural region
	Hyderabad	17.48º N	78.40º E	545	6.81	ICARB	BC	In central Indian Peninsula
	Pune	18.52º N	73.85º E	559	5.05	ICARB	BC	In western plateau
	Kanpur	26.51º N	80.23 ºE	123	2.77	AERONET/ ISRO-GBP	Misc.[d]	In central IGP
	Agra	27.06º N	78.03º E	169	1.75	ISRO-GBP	Misc.[d]	Between Delhi and Kanpur
	Allahabad	25.45º N	81.85º E	98	1.22	ISRO-GBP	Misc.[d]	In central-eastern IGP
Semi-Urban	Kharagpur	22.52º N	87.52º E	28	0.37	ICARB	BC	In eastern IGP-outflow region to Bay of Bengal
	Hisar	29.09º N	75.42º E	41	0.3	ISRO-GBP	Misc.[d]	Surrounded by agricultural field in western IGP
	Trivandrum	8.55º N	76.90º E	3	0.75	ICARB	BC	A coastal station in southern India
Remote	Port Blair	11.63º N	92.70º E	60	0.1	ICARB	BC	Island in Bay of Bengal
	Nainital	29.20º N	79.30º E	1950	0.04	ICARB	BC	High altitude remote location in the Himalayan foothills
	Minicoy	8.30º N	70.00º E	1	0.009	ICARB	BC	Island in Arabian Sea

[a] In decreasing order of the population
[b] Statistics in 2011 from wikipedia
[c] Details in section 3.2 and 3.3
[d] Miscellaneous, including meteorological fields, AOD, AAOD and aerosol surface concentration.

Table 3. The statistics of the aerosol parameters over South Asia (60°E–95°E; 5°N–36°N. Land only) in 2006.

Parameter	Unit	#	Mean	Median	Min	Max	Stdev	Diversity [a]
				SO_4				
Emi [b]	Tg(SO_2) yr^{-1}	7	7.36	7.39	5.81	8.61	0.86	12%
Cheaq[c]	Tg(SO_4) yr^{-1}	4	0.27	0.28	0.15	0.35	0.10	36%
Cheg[d]	Tg(SO_4) yr^{-1}	4	0.24	0.18	0.12	0.46	0.16	**66%** [h]
Wet	Tg(SO_4) yr^{-1}	7	4.38	3.98	3.64	6.21	0.93	21%
Dry	Tg(SO_4) yr^{-1}	7	0.78	0.77	0.27	1.26	0.35	**44%**
Dry/Dry+Wet	%	7	19	20	8	29	8	40%
Life time	Days	7	5.02	4.81	3.22	8.50	1.73	34%
Load	Tg(SO_4)	7	0.06	0.05	0.04	0.08	0.02	26%
MEE[e]	m^2 g^{-1}(SO_4)	4	8.56	8.99	5.58	10.68	2.15	25%
AOD	Unitless	4	0.07	0.07	0.04	0.08	0.02	27%
				BC				
Emi	Tg yr^{-1}	7	0.70	0.71	0.59	0.78	0.06	9%
Wet	Tg yr^{-1}	7	0.27	0.28	0.21	0.31	0.04	15%
Dry	Tg yr^{-1}	7	0.15	0.19	0.05	0.21	0.07	46%
Dry/Dry+Wet	%	7	33	37	15	41	10	29%
Life time	Days	7	7.67	6.56	4.13	15.82	3.84	**50%**
Load	Tg	7	0.008	0.007	0.005	0.014	0.003	39%
MEE	m^2 g^{-1}	4	7.07	7.56	2.77	10.40	3.63	**51%**
AOD	Unitless	4	0.008	0.010	0.003	0.011	0.004	45%
				OA				
Emi[f]	Tg yr^{-1}	7	3.69	3.58	2.77	4.46	0.61	16%
Wet	Tg yr^{-1}	7	1.68	1.62	1.26	2.31	0.37	22%
Dry	Tg yr^{-1}	7	0.78	0.82	0.31	1.21	0.32	**41%**
Dry/Dry+Wet	%	7	35	38	20	44	10	**29%**
Life time	Days	7	5.60	5.25	4.44	7.09	1.07	19%
Load	Tg	7	0.05	0.04	0.03	0.07	0.01	25%
MEE	m^2 g^{-1}	4	5.17	4.99	3.69	7.00	1.39	27%
AOD	Unitless	4	0.023	0.022	0.018	0.030	0.005	21%
				DUST				
Emi	Tg yr^{-1}	7	103.84	43.34	6.43	367.28	128.23	**124%**
Wet	Tg yr^{-1}	7	43.43	41.07	11.82	92.55	24.47	56%
Dry + Sed[g]	Tg yr^{-1}	7	98.50	46.92	1.34	316.87	113.42	**115%**
Dry/Dry+Wet	%	7	56	68	12	84	26	47%
Life time	Days	7	3.86	4.17	1.08	6.92	1.98	51%
Load	Tg	7	0.87	0.91	0.16	1.43	0.39	45%
MEE	m^2 g^{-1}	4	0.64	0.59	0.50	0.89	0.17	27%
AOD	Unitless	4	0.10	0.09	0.08	0.12	0.02	22%
				TOTAL				
AOD	Unitless	7	0.21	0.18	0.16	0.33	0.06	28%
AAOD	Unitless	7	0.02	0.02	0.01	0.02	0.01	37%

[a]. The diversity is defined as the ratio of standard deviation and mean (i.e. stdev/mean). The largest and second largest diversities in each species are highlighted in bold.
[b]. The emission of SO_2, including anthropogenic and biomass burning emission.
[c]. The chemical production of SO_4 in aqueous phase reaction (i.e. SO_2 reacts with H_2O_2).
[d]. The chemical production of SO_4 in gaseous phase reaction (i.e. SO_2 reacts with OH).
[e]. Mass extinction efficiency, defined as the ratio of AOD and load (i.e. AOD/load).
[f]. Sum of anthropogenic emission, biomass burning emissions and secondary organic aerosol.
[g]. Dry deposition plus sedimentation.
[h]. The top two largest diversities in each species are highlighted in bold.

Figures

Captions

Fig. 1. Topography of South Asia and the locations of the stations used in this study. Three AERONET stations are labeled in blue, eight ICARB stations in red, and four ISRO-GBP stations in black except for Kanpur. The topography map is obtained from http://mapofasia.blogspot.com/2013/02/map-of-south-asia-area-pictures.html.

Fig. 2. Spatial distribution of anthropogenic emissions of BC, OC, SO_2, NH_3 and NO_x averaged for 2000-2007 from A2-ACCMIP emission dataset (units: g m^{-2} yr^{-1}) over South Asia (60°E–95°E; 5°N –36°N). The annual mean emission amount over South Asia (land only) is shown at the bottom.

Fig. 3. Spatial distribution of biomass burning emission of BC based on GFED2 for each season averaged for 2000-2007 (units: g C m^{-2} yr^{-1}) over South Asia (60°E–95°E; 5°N –36°N). The seasonal mean emission amount over South Asia (land only) is shown at the bottom. Note that the color scale is the same as that of BC in the Fig. 2 for the purpose of comparison.

Fig. 4. The annual averaged mean AOD for 2000-2007 over region: (a) South Asia (60°E–95°E; 5°N –36°N, averaged over land only, i.e. the gray area in the map); (b) Central IGP (77°E-83°E; 25°N-28°N, averaged over the red box on the map shown in Fig. 4a). Thin lines with symbols represent seven models, and thick lines represent four satellite datasets. Multi-year averaged mean AOD and the standard deviation is listed on each panel.

Fig. 5. Monthly mean AOD (left column) and AAOD (right column) at three AERONET stations in South Asia. The gray bar represents data from AERONET, the thin lines represent results from seven models, and symbols represent the data from three satellite retrievals. On each panel, corr is correlation coefficient of a model with AERONET, bias is relative mean bias, i.e. Σ (AOD_MODEL_i)/Σ ($AOD\_AERONET_i$), and rmse is root-mean-square error relative to AERONET.

Fig. 6. Monthly AOD of total aerosol (aer) and components (ss, so_4, bc, oa, dust, no_3, soa and bb) at Kanpur in 2004 from four models, HAD (upper left), GOC (upper right), GE5 (lower left), and SPR (lower right). The gray bar represents total AOD from AERONET, and the lines represent the model results of total AOD (black line) and component AODs (colored lines). The corresponding annual mean values are also listed. NOTE: For the HAD model, bc and oa are only from fossil fuel sources; the biomass burning aerosol is labeled "bb".

Fig. 7a. Spatial distribution of AOD over South Asia in four seasons averaged for 2000–2007 from four satellite datasets (MODIS-Terra, MODIS-Aqua, MISR, and SeaWiFS). The corresponding area averaged seasonal mean AOD value over land is listed on each panel. Three AERONET stations used in this study are labeled in the maps for references. Area in white means no retrieval available due to the presence of bright surface or frequent cloud cover.

Fig. 7b. Spatial distribution of AOD over South Asia in four seasons averaged for 2000–2007 from seven models (the first three models using the anthropogenic emissions from A2-MAP and the rest using A2-ACCMIP). The area averaged seasonal mean AOD value over land is listed on each panel. Three AERONET stations used in this study are shown on the maps for references.

Fig. 8. Seasonal mean of vertical profile of extinction coefficient (units: km^{-1}) at (a) Kanpur, and (b) Hyderabad from CALIOP and seven models. The corresponding seasonal mean AOD, Za (units: km) and F_{2km} are listed after each symbol name. The gray shaded area in CALIOP is one standard deviation relative to the average of 2006-2011.

Fig. 9. Monthly mean surface BC concentration at eight ICARB stations in 2006 (units: $\mu g\ m^{-3}$). Gray bar represents measurement from ICARB and thin lines represent seven models.

Fig.10. Comparisons of seven models against ISRO-GBP campaign measurements at four IGP stations (Hisar, Agra, Kanpur, Allahabad from western to eastern IGP) in December 2004. The variables include meteorological fields of surface relative humidity (1st row) and surface temperature (2nd row), aerosol species mass concentrations of SO_4^{2-} (3rd row), NO_3^- (4th row), BC (5th row), and OA (6th row), and columnar AOD (7th row) and AAOD (8th row) at 550nm.

Fig. 11. Mass extinction efficiency (MEE) at 550nm for individual aerosol components (units: $m^2\ g^{-1}$) as a function of relative humidity (RH). For SO_4^{2-}, OC and BC, MEE is calculated using the relationship of RH and size growth based on optical properties of aerosols and clouds (OPAC) (Hess et al., 1998). For NO_3^-, MEE is calculated according to the work by A. Lacis (http://gacp.giss.nasa.gov/data_sets/lacis/introduction.pdf).

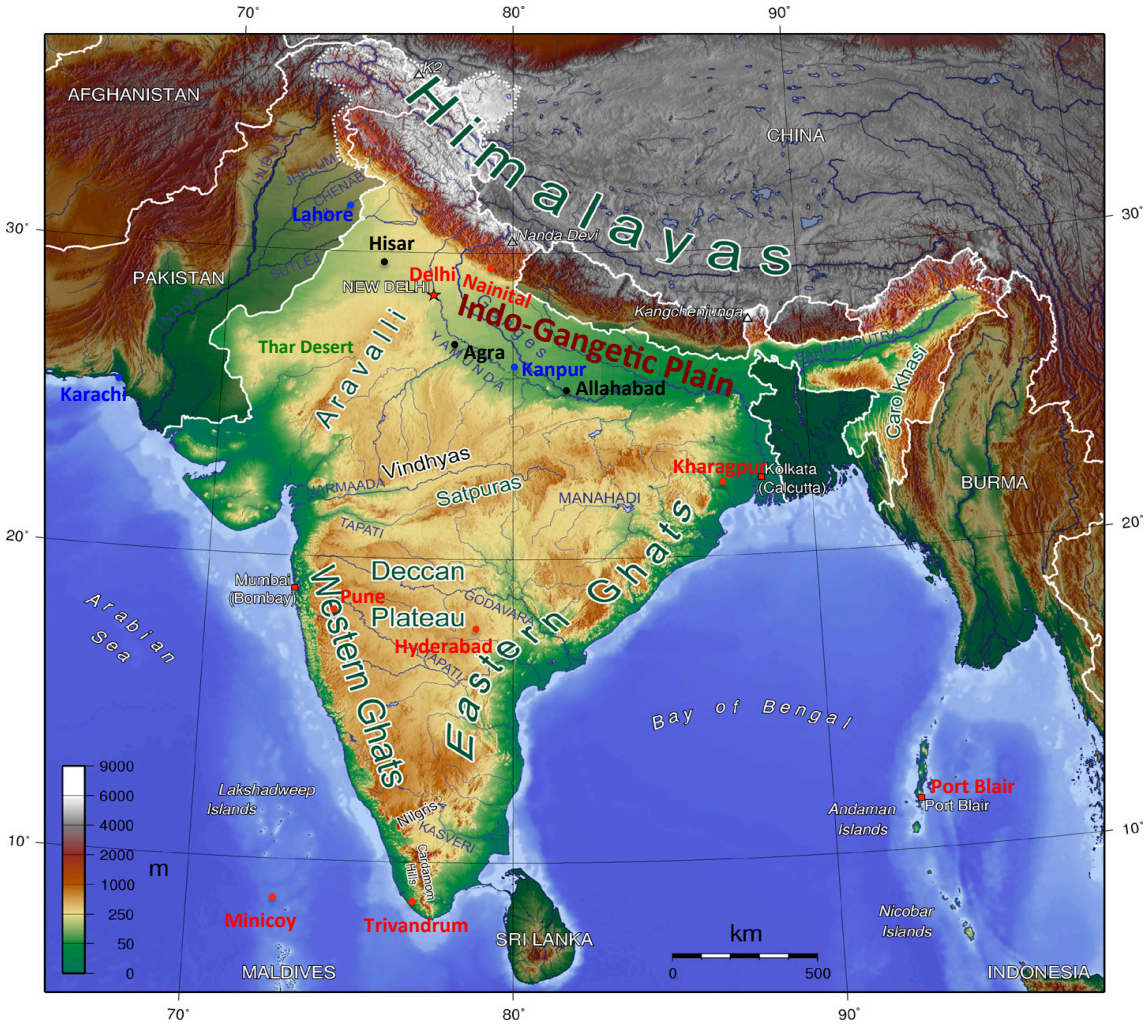
70°
80°
90°
30°
20°
10°
AFGHANISTAN
PAKISTAN
CHINA
BURMA
INDONESIA
SRI LANKA
MALDIVES
Himalayas
K2
Nanda Devi
Kangchenjunga
Indo-Gangetic Plain
Thar Desert
Aravalli
Vindhyas
Satpuras
MANAHADI
Deccan
Plateau
Eastern Ghats
Western Ghats
Arabian Sea
Bay of Bengal
Lahore
Hisar
Delhi
NEW DELHI
Nainital
Agra
Kanpur
Allahabad
Karachi
Kharagpur
Kolkata
(Calcutta)
Mumbai
(Bombay)
Pune
Hyderabad
Port Blair
Port Blair
Andaman
Islands
Nicobar
Islands
Lakshadweep
Islands
Minicoy
Trivandrum
Cardamom
Hills
Caro Khasi
INDUS
JHELUM
CHENAB
SUTLEJ
GANGES
YAMUNA
NARMADA
TAPATI
GODAVARI
KRISHNA
KAVERI
Nilgris
9000
6000
4000
2000
1000
250
50
0
m
km
0
500

Fig. 1.

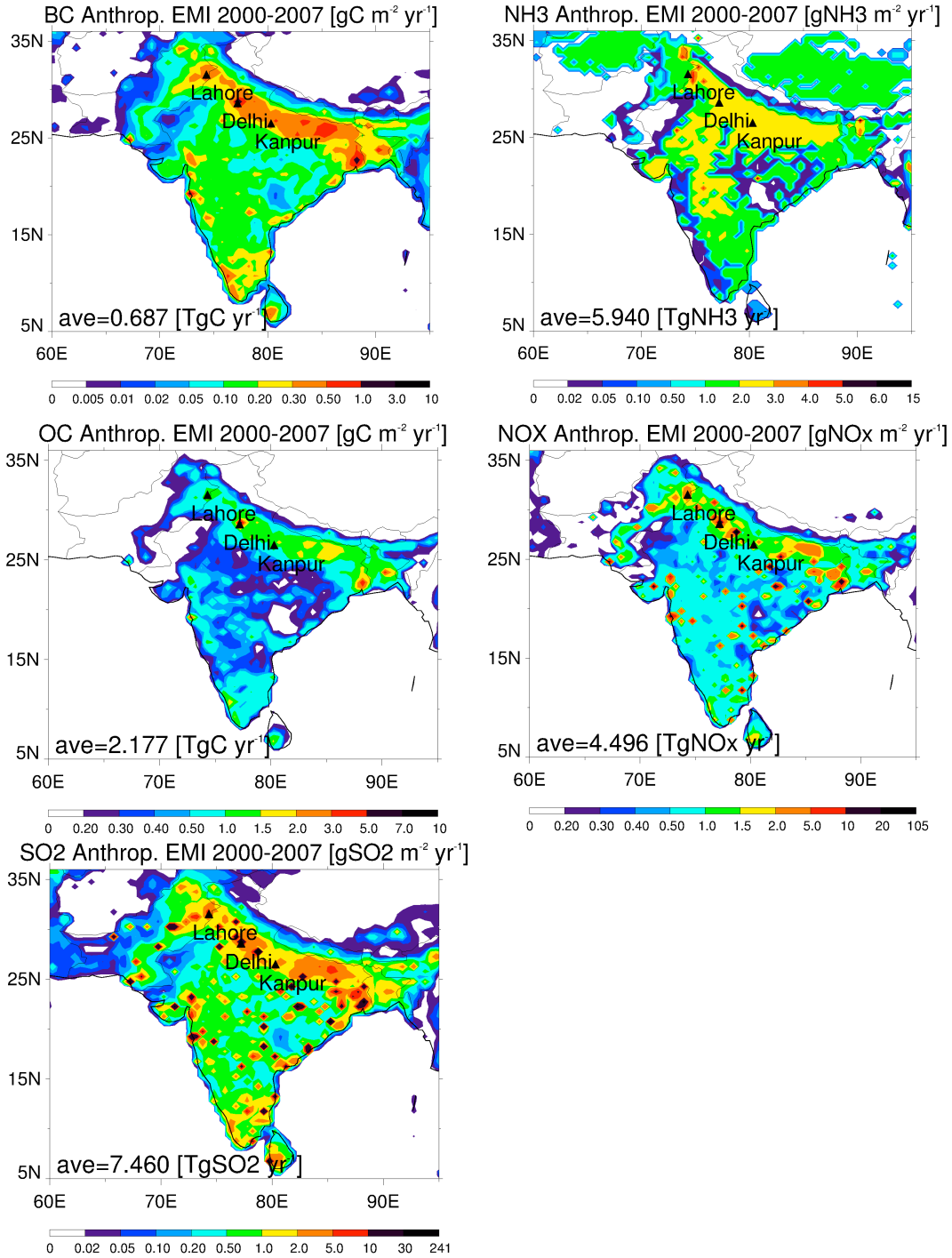
BC Anthrop. EMI 2000-2007 [gC m-2 yr-1]
Lahore
Delhi
Kanpur
ave=0.687 [TgC yr-1]
0 0.005 0.01 0.02 0.05 0.10 0.20 0.30 0.50 1.0 3.0 10
NH3 Anthrop. EMI 2000-2007 [gNH3 m-2 yr-1]
ave=5.940 [TgNH3 yr-1]
0 0.02 0.05 0.10 0.50 1.0 2.0 3.0 4.0 5.0 6.0 15
OC Anthrop. EMI 2000-2007 [gC m-2 yr-1]
ave=2.177 [TgC yr-1]
0 0.20 0.30 0.40 0.50 1.0 1.5 2.0 3.0 5.0 7.0 10
NOX Anthrop. EMI 2000-2007 [gNOx m-2 yr-1]
ave=4.496 [TgNOx yr-1]
0 0.20 0.30 0.40 0.50 1.0 1.5 2.0 5.0 10 20 105
SO2 Anthrop. EMI 2000-2007 [gSO2 m-2 yr-1]
ave=7.460 [TgSO2 yr-1]
0 0.02 0.05 0.10 0.20 0.50 1.0 2.0 5.0 10 30 241
35N
25N
15N
5N
60E
70E
80E
90E

Fig. 2.

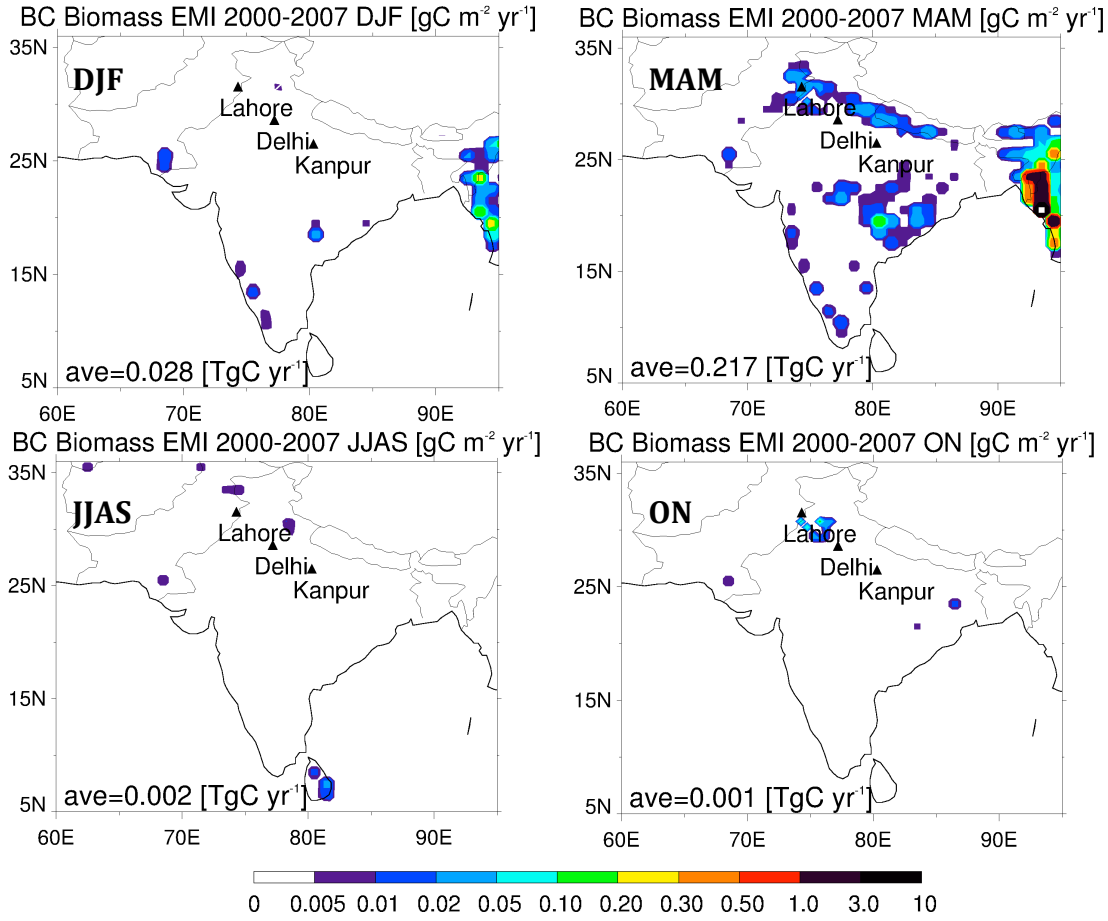
BC Biomass EMI 2000-2007 DJF [gC m-2 yr-1]
DJF
Lahore
Delhi
Kanpur
ave=0.028 [TgC yr-1]
BC Biomass EMI 2000-2007 MAM [gC m-2 yr-1]
MAM
Lahore
Delhi
Kanpur
ave=0.217 [TgC yr-1]
BC Biomass EMI 2000-2007 JJAS [gC m-2 yr-1]
JJAS
Lahore
Delhi
Kanpur
ave=0.002 [TgC yr-1]
BC Biomass EMI 2000-2007 ON [gC m-2 yr-1]
ON
Lahore
Delhi
Kanpur
ave=0.001 [TgC yr-1]
35N
25N
15N
5N
60E
70E
80E
90E
0 0.005 0.01 0.02 0.05 0.10 0.20 0.30 0.50 1.0 3.0 10

Fig. 3.

320

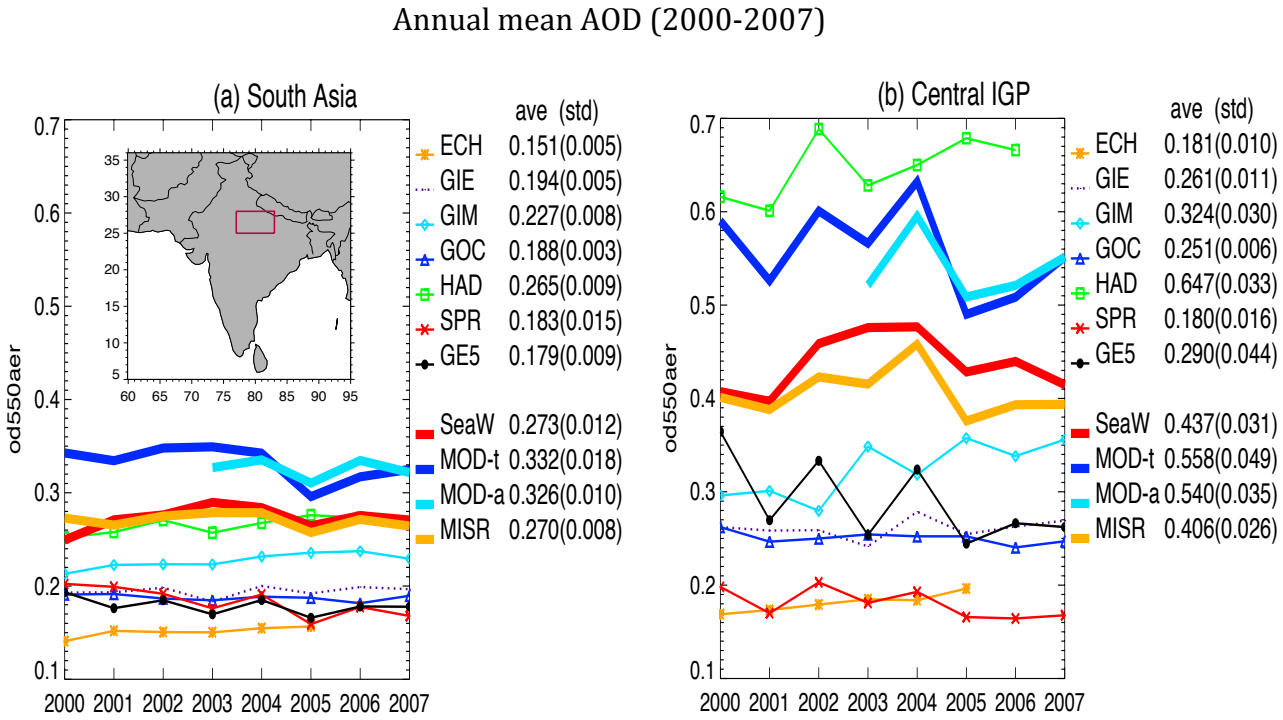

321 Fig. 4.
322

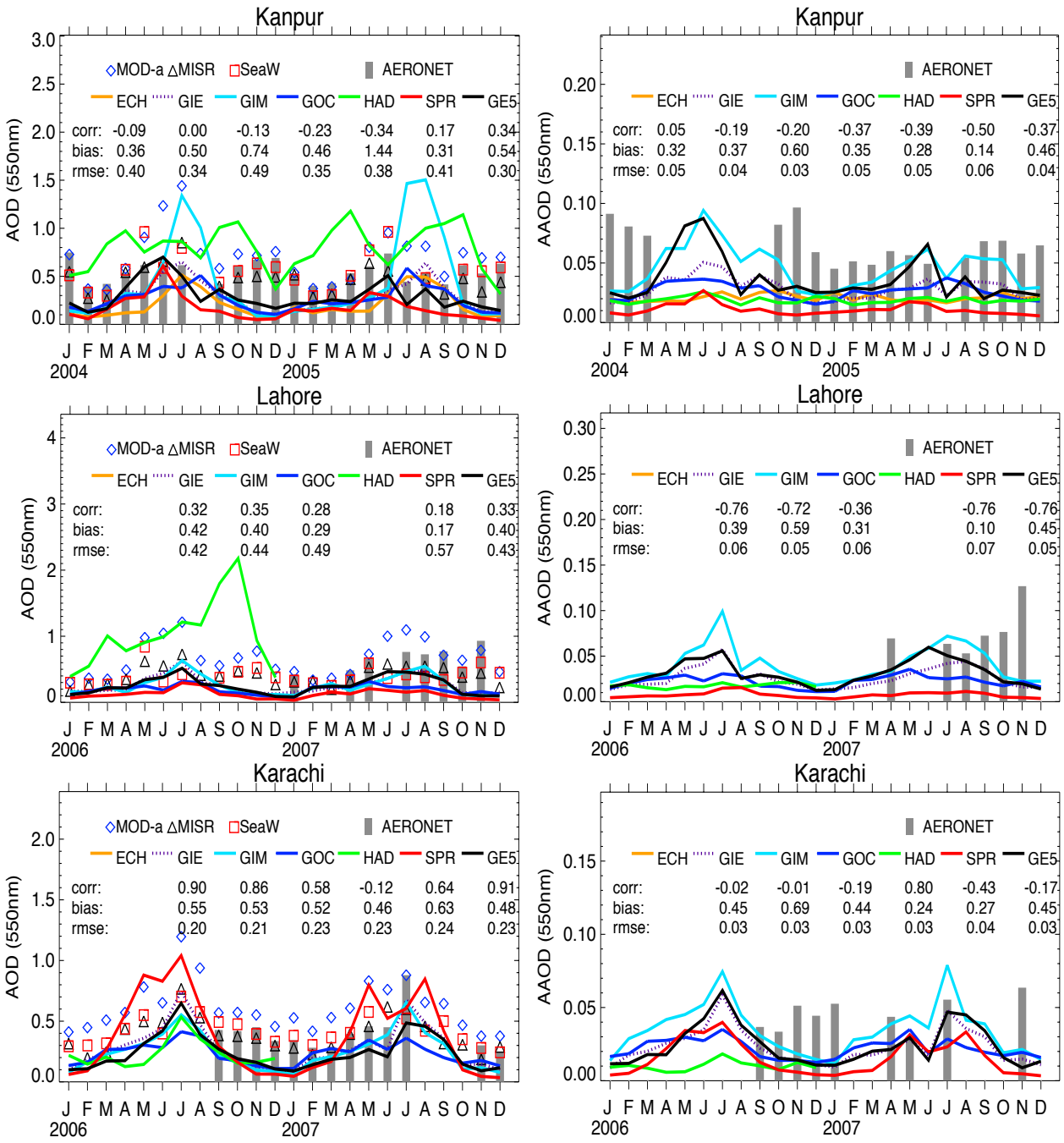
Kanpur
MOD-a △MISR □SeaW AERONET
ECH GIE GIM GOC HAD SPR GE5
corr: -0.09 0.00 -0.13 -0.23 -0.34 0.17 0.34
bias: 0.36 0.50 0.74 0.46 1.44 0.31 0.54
rmse: 0.40 0.34 0.49 0.35 0.38 0.41 0.30
AOD (550nm)
AAOD (550nm)
corr: 0.05 -0.19 -0.20 -0.37 -0.39 -0.50 -0.37
bias: 0.32 0.37 0.60 0.35 0.28 0.14 0.46
rmse: 0.05 0.04 0.03 0.05 0.05 0.06 0.04
Lahore
corr: 0.32 0.35 0.28 0.18 0.33
bias: 0.42 0.40 0.29 0.17 0.40
rmse: 0.42 0.44 0.49 0.57 0.43
corr: -0.76 -0.72 -0.36 -0.76 -0.76
bias: 0.39 0.59 0.31 0.10 0.45
rmse: 0.06 0.05 0.06 0.07 0.05
Karachi
corr: 0.90 0.86 0.58 -0.12 0.64 0.91
bias: 0.55 0.53 0.52 0.46 0.63 0.48
rmse: 0.20 0.21 0.23 0.23 0.24 0.23
corr: -0.02 -0.01 -0.19 0.80 -0.43 -0.17
bias: 0.45 0.69 0.44 0.24 0.27 0.45
rmse: 0.03 0.03 0.03 0.03 0.04 0.03
J F M A M J J A S O N D J F M A M J J A S O N D
2004 2005
2006 2007

Fig. 5.

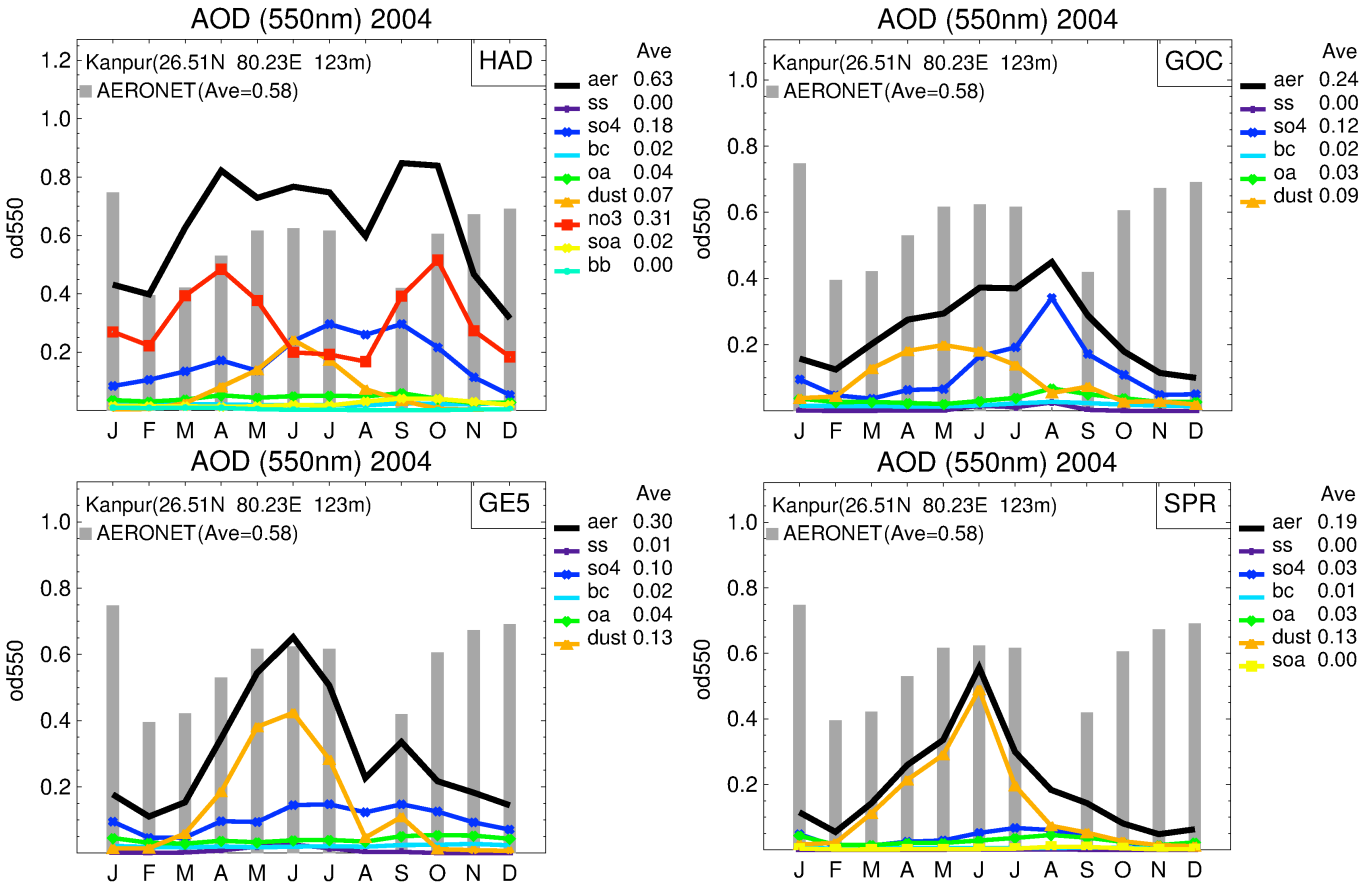
AOD (550nm) 2004
Kanpur(26.51N 80.23E 123m)
AERONET(Ave=0.58)
HAD
Ave
aer 0.63
ss 0.00
so4 0.18
bc 0.02
oa 0.04
dust 0.07
no3 0.31
soa 0.02
bb 0.00
GOC
aer 0.24
ss 0.00
so4 0.12
bc 0.02
oa 0.03
dust 0.09
GE5
aer 0.30
ss 0.01
so4 0.10
bc 0.02
oa 0.04
dust 0.13
SPR
aer 0.19
ss 0.00
so4 0.03
bc 0.01
oa 0.03
dust 0.13
soa 0.00
od550
J F M A M J J A S O N D

Fig. 6.

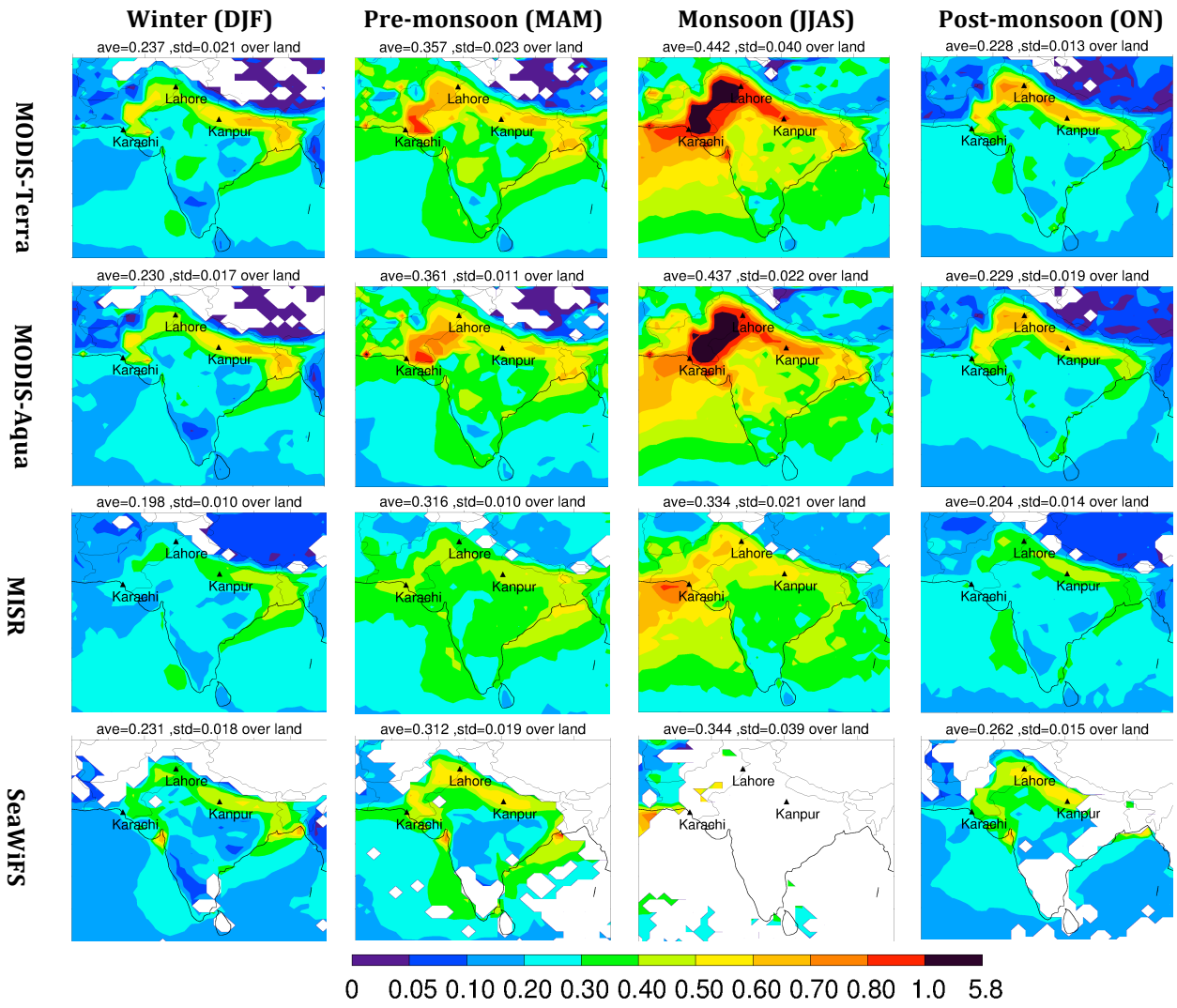
Winter (DJF)
Pre-monsoon (MAM)
Monsoon (JJAS)
Post-monsoon (ON)
MODIS-Terra
MODIS-Aqua
MISR
SeaWiFS
ave=0.237 ,std=0.021 over land
ave=0.357 ,std=0.023 over land
ave=0.442 ,std=0.040 over land
ave=0.228 ,std=0.013 over land
ave=0.230 ,std=0.017 over land
ave=0.361 ,std=0.011 over land
ave=0.437 ,std=0.022 over land
ave=0.229 ,std=0.019 over land
ave=0.198 ,std=0.010 over land
ave=0.316 ,std=0.010 over land
ave=0.334 ,std=0.021 over land
ave=0.204 ,std=0.014 over land
ave=0.231 ,std=0.018 over land
ave=0.312 ,std=0.019 over land
ave=0.344 ,std=0.039 over land
ave=0.262 ,std=0.015 over land
Lahore
Kanpur
Karachi
0 0.05 0.10 0.20 0.30 0.40 0.50 0.60 0.70 0.80 1.0 5.8

Fig. 7a

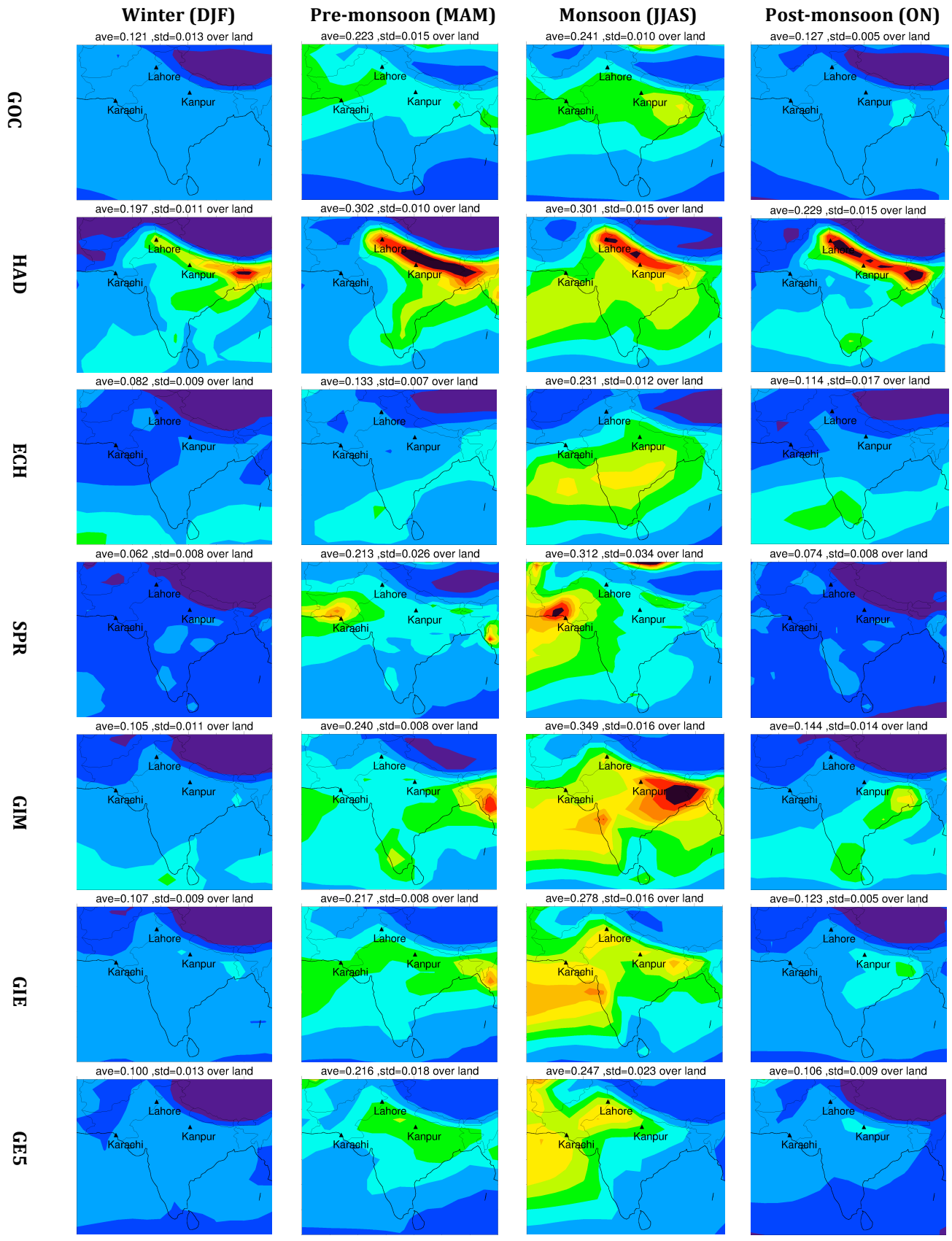
Winter (DJF)
Pre-monsoon (MAM)
Monsoon (JJAS)
Post-monsoon (ON)
GOC
HAD
ECH
SPR
GIM
GIE
GE5
ave=0.121 ,std=0.013 over land
ave=0.223 ,std=0.015 over land
ave=0.241 ,std=0.010 over land
ave=0.127 ,std=0.005 over land
ave=0.197 ,std=0.011 over land
ave=0.302 ,std=0.010 over land
ave=0.301 ,std=0.015 over land
ave=0.229 ,std=0.015 over land
ave=0.082 ,std=0.009 over land
ave=0.133 ,std=0.007 over land
ave=0.231 ,std=0.012 over land
ave=0.114 ,std=0.017 over land
ave=0.062 ,std=0.008 over land
ave=0.213 ,std=0.026 over land
ave=0.312 ,std=0.034 over land
ave=0.074 ,std=0.008 over land
ave=0.105 ,std=0.011 over land
ave=0.240 ,std=0.008 over land
ave=0.349 ,std=0.016 over land
ave=0.144 ,std=0.014 over land
ave=0.107 ,std=0.009 over land
ave=0.217 ,std=0.008 over land
ave=0.278 ,std=0.016 over land
ave=0.123 ,std=0.005 over land
ave=0.100 ,std=0.013 over land
ave=0.216 ,std=0.018 over land
ave=0.247 ,std=0.023 over land
ave=0.106 ,std=0.009 over land
Lahore
Kanpur
Karachi
0 0.05 0.10 0.20 0.30 0.40 0.50 0.60 0.70 0.80 1.0 5.8

Fig.7b.

350

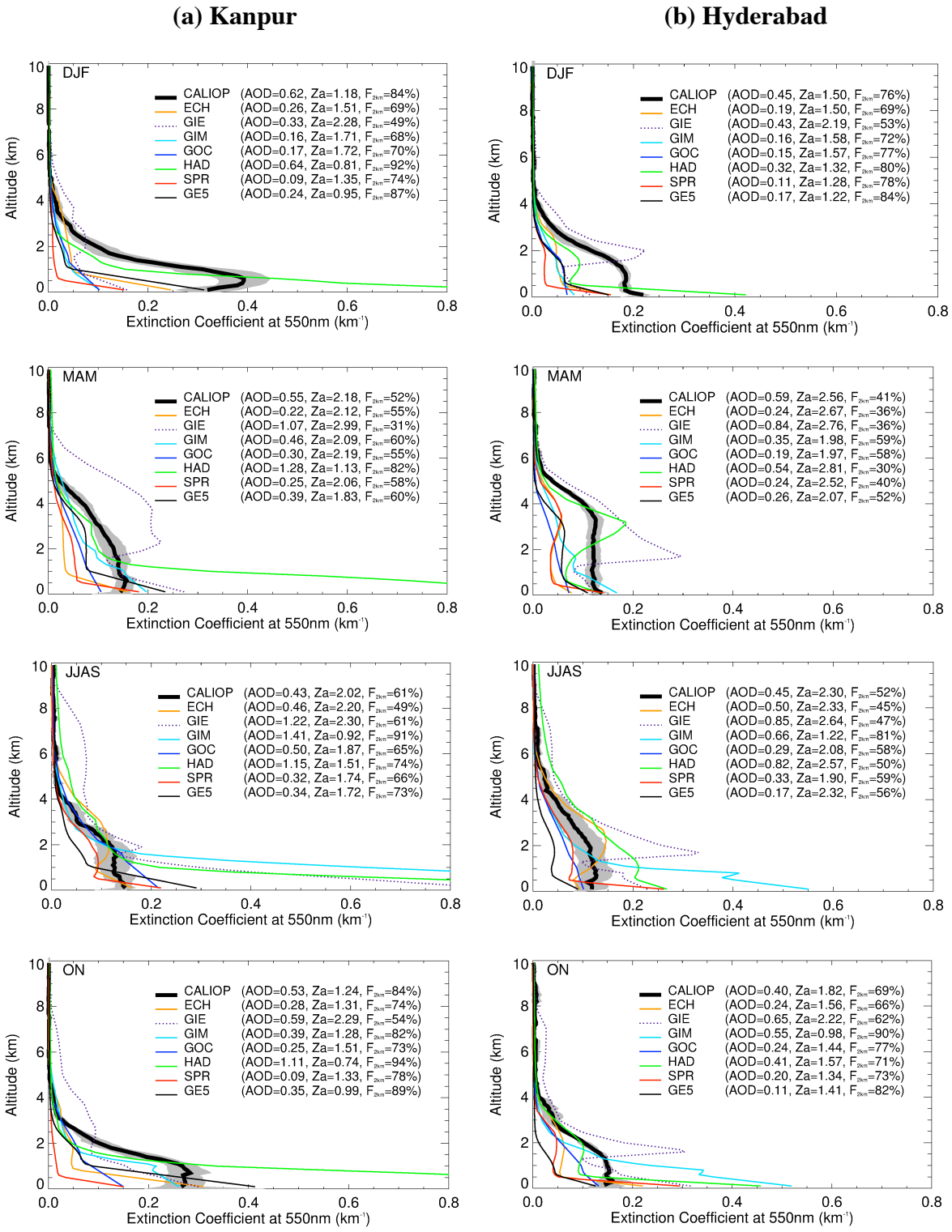
(a) Kanpur
(b) Hyderabad
DJF
CALIOP (AOD=0.62, Za=1.18, F2km=84%)
ECH (AOD=0.26, Za=1.51, F2km=69%)
GIE (AOD=0.33, Za=2.28, F2km=49%)
GIM (AOD=0.16, Za=1.71, F2km=68%)
GOC (AOD=0.17, Za=1.72, F2km=70%)
HAD (AOD=0.64, Za=0.81, F2km=92%)
SPR (AOD=0.09, Za=1.35, F2km=74%)
GE5 (AOD=0.24, Za=0.95, F2km=87%)
DJF
CALIOP (AOD=0.45, Za=1.50, F2km=76%)
ECH (AOD=0.19, Za=1.50, F2km=69%)
GIE (AOD=0.43, Za=2.19, F2km=53%)
GIM (AOD=0.16, Za=1.58, F2km=72%)
GOC (AOD=0.15, Za=1.57, F2km=77%)
HAD (AOD=0.32, Za=1.32, F2km=80%)
SPR (AOD=0.11, Za=1.28, F2km=78%)
GE5 (AOD=0.17, Za=1.22, F2km=84%)
MAM
CALIOP (AOD=0.55, Za=2.18, F2km=52%)
ECH (AOD=0.22, Za=2.12, F2km=55%)
GIE (AOD=1.07, Za=2.99, F2km=31%)
GIM (AOD=0.46, Za=2.09, F2km=60%)
GOC (AOD=0.30, Za=2.19, F2km=55%)
HAD (AOD=1.28, Za=1.13, F2km=82%)
SPR (AOD=0.25, Za=2.06, F2km=58%)
GE5 (AOD=0.39, Za=1.83, F2km=60%)
MAM
CALIOP (AOD=0.59, Za=2.56, F2km=41%)
ECH (AOD=0.24, Za=2.67, F2km=36%)
GIE (AOD=0.84, Za=2.76, F2km=36%)
GIM (AOD=0.35, Za=1.98, F2km=59%)
GOC (AOD=0.19, Za=1.97, F2km=58%)
HAD (AOD=0.54, Za=2.81, F2km=30%)
SPR (AOD=0.24, Za=2.52, F2km=40%)
GE5 (AOD=0.26, Za=2.07, F2km=52%)
JJAS
CALIOP (AOD=0.43, Za=2.02, F2km=61%)
ECH (AOD=0.46, Za=2.20, F2km=49%)
GIE (AOD=1.22, Za=2.30, F2km=61%)
GIM (AOD=1.41, Za=0.92, F2km=91%)
GOC (AOD=0.50, Za=1.87, F2km=65%)
HAD (AOD=1.15, Za=1.51, F2km=74%)
SPR (AOD=0.32, Za=1.74, F2km=66%)
GE5 (AOD=0.34, Za=1.72, F2km=73%)
JJAS
CALIOP (AOD=0.45, Za=2.30, F2km=52%)
ECH (AOD=0.50, Za=2.33, F2km=45%)
GIE (AOD=0.85, Za=2.64, F2km=47%)
GIM (AOD=0.66, Za=1.22, F2km=81%)
GOC (AOD=0.29, Za=2.08, F2km=58%)
HAD (AOD=0.82, Za=2.57, F2km=50%)
SPR (AOD=0.33, Za=1.90, F2km=59%)
GE5 (AOD=0.17, Za=2.32, F2km=56%)
ON
CALIOP (AOD=0.53, Za=1.24, F2km=84%)
ECH (AOD=0.28, Za=1.31, F2km=74%)
GIE (AOD=0.59, Za=2.29, F2km=54%)
GIM (AOD=0.39, Za=1.28, F2km=82%)
GOC (AOD=0.25, Za=1.51, F2km=73%)
HAD (AOD=1.11, Za=0.74, F2km=94%)
SPR (AOD=0.09, Za=1.33, F2km=78%)
GE5 (AOD=0.35, Za=0.99, F2km=89%)
ON
CALIOP (AOD=0.40, Za=1.82, F2km=69%)
ECH (AOD=0.24, Za=1.56, F2km=66%)
GIE (AOD=0.65, Za=2.22, F2km=62%)
GIM (AOD=0.55, Za=0.98, F2km=90%)
GOC (AOD=0.24, Za=1.44, F2km=77%)
HAD (AOD=0.41, Za=1.57, F2km=71%)
SPR (AOD=0.20, Za=1.34, F2km=73%)
GE5 (AOD=0.11, Za=1.41, F2km=82%)
Altitude (km)
Extinction Coefficient at 550nm (km-1)

351 Fig. 8.

352

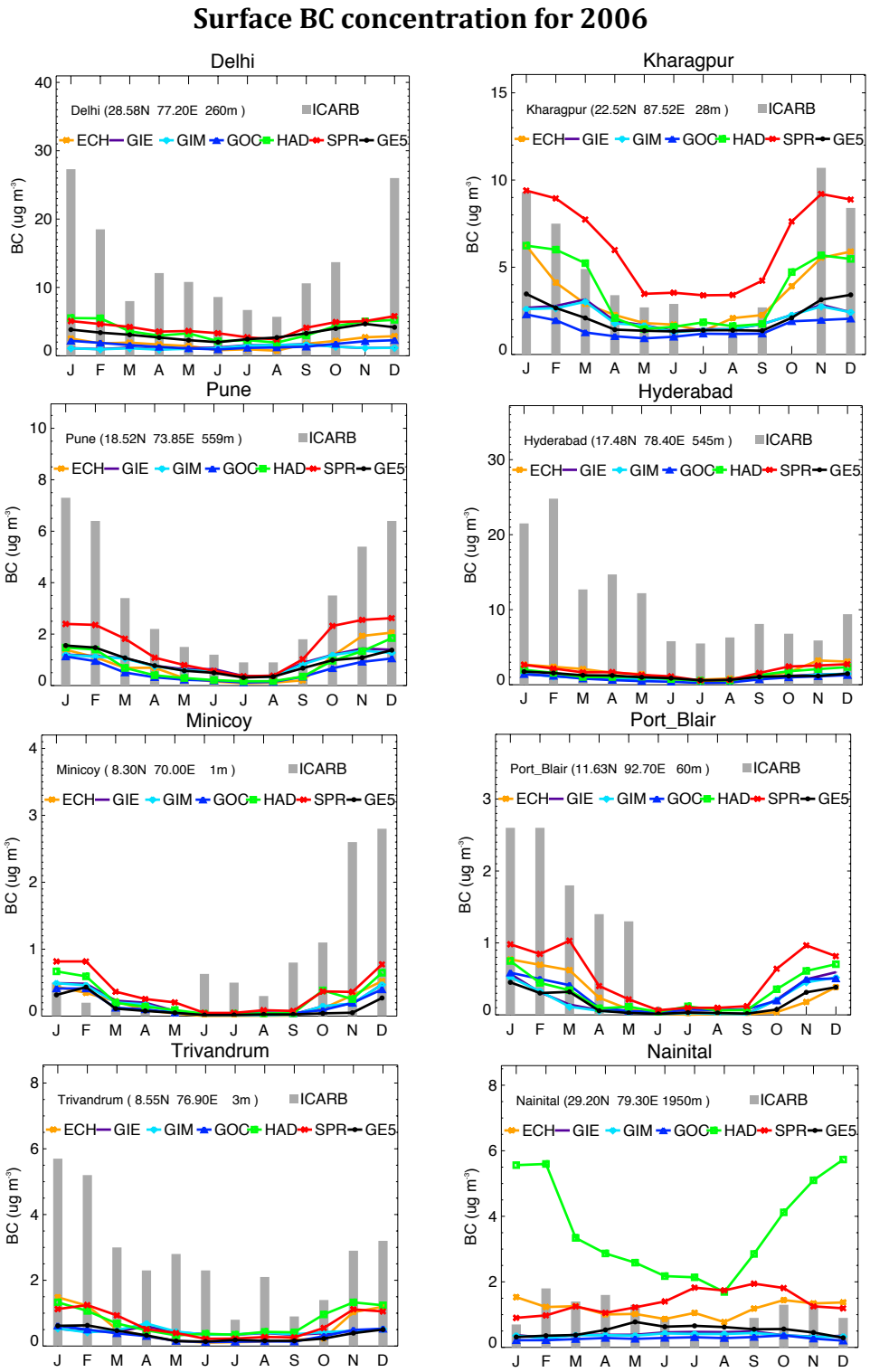

353

354 Fig. 9.

355

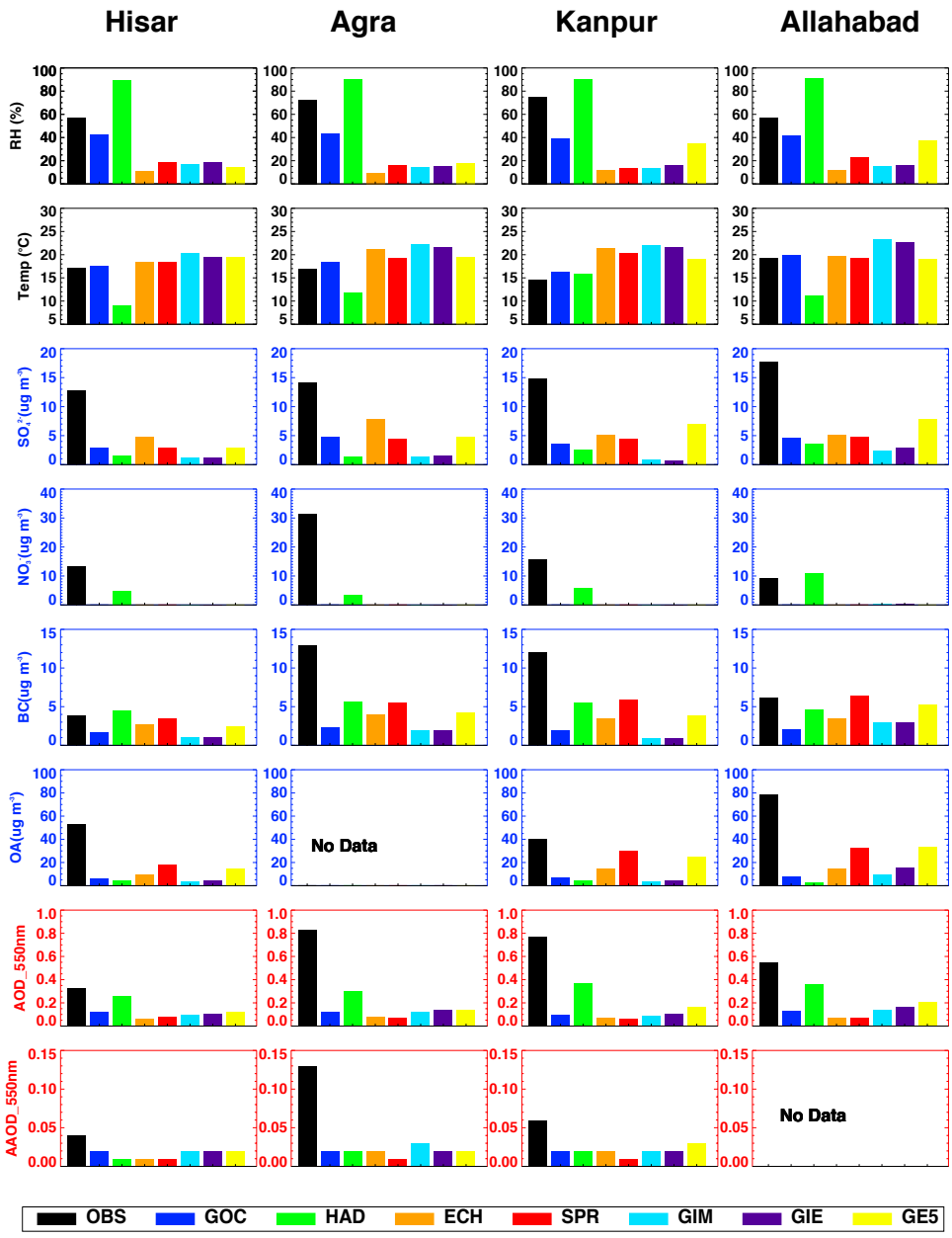
Hisar
Agra
Kanpur
Allahabad
RH (%)
Temp (°C)
No Data
No Data
OBS
GOC
HAD
ECH
SPR
GIM
GIE
GE5

Fig.10.

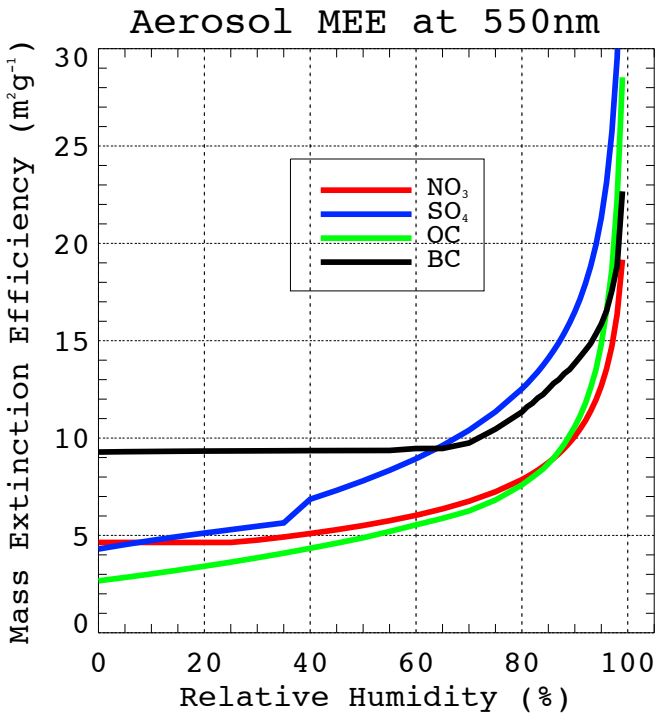
Aerosol MEE at 550nm
Mass Extinction Efficiency (m²g⁻¹)
Relative Humidity (%)
NO3
SO4
OC
BC
0
5
10
15
20
25
30
0
20
40
60
80
100

Fig. 11.